Supplementary Information

"Impurity"-driven Tunable Organic Room Temperature Phosphorescence via Conformational Regulation in Multi Host/Guest Systems

Arnab Dutta,[a] Utkarsh Singh,[b] Swapan K. Pati,[b]* and Uday Maitra[a]*

[a]Department of Organic Chemistry, Indian Institute of Science, Bengaluru 560012, Karnataka, India.
[b]Theoretical Sciences Unit, School of Advanced Materials (SAMat), Jawaharlal Nehru Centre for Advanced Scientific Research, Bengaluru 560064, Karnataka, India.

1. Materials and methods: Biphenyl, 4-methoxycarbonylphenylboronic acid, triphenylphosphine, tertrakis(triphenylphosphine)palladium(0), palladium(II) chloride, naphthalene, anthracene and poly(methyl methacrylate) were purchased from Sigma Aldrich. Phenylboronic acid, 4-iodobenzoic acid, oxalyl chloride, aluminium chloride and carbon disulfide were procured from Spectrochem. Succinic acid, palmitic acid, benzoic acid, sodium hydroxide, potassium hydroxide, potassium carbonate, anhydrous sodium sulfate and solvents were purchased from S. D. Fine Chemicals Ltd. 4,4'-Dibromobenzil and benzophenone were obtained from Alfa Aesar and Nice Chemical Ltd., respectively. Commercial biphenyl-4-carboxylic acid (**com-BCA**) was procured from Sigma Aldrich. Commercial biphenyl-4,4'-dicarboxylic acid (**com-BDCA**) was sourced from Sigma Aldrich and Fluka. All the hosts used in the study were recrystallized from the appropriate distilled solvent. MiliQ water (18.2 MΩ·cm at 25 °C) was used for all the experiments. NMR spectra were recorded in a Bruker UltraShield 400 MHz spectrometer. Chemical shifts are reported in δ (ppm) relative to solvent residual peak (δ = 7.26 and 77.1 ppm for ^{1}H and ^{13}C, respectively, in $CDCl_3$, and δ = 2.50 and 39.5 ppm for ^{1}H and ^{13}C, respectively, in DMSO-D_6). Multiplicities are reported as follows: s (singlet), d (doublet), dd (doublet of doublets), t (triplet) and m (multiplet). Coupling constants (*J*) are reported in Hertz (Hz), and 'nH' indicates the number (n) of protons associated with a given signal. A Xevo G2-XS QTof instrument was used to acquire high-resolution mass spectra (HRMS). IR spectra were acquired in a Bruker Alpha FTIR instrument. Absorption spectra were recorded on a UV-2600i Shimadzu UV-Vis-NIR spectrometer. All the room temperature (298 K) photoluminescence measurements including RTP quantum yield and lifetime measurements were carried out on an Edinburgh FLS980 fluorimeter. Fluorescence lifetime measurements were done on an Edinburgh FLS920 instrument using a nanosecond laser. Photoluminescence measurements at cryogenic temperatures (77 K) were carried out on an Edinburgh FLS1000 fluorimeter. High-performance liquid chromatography (HPLC) analysis was carried out using a Shimadzu UFLC HPLC system equipped with a gradient pump and PDA detector. A Shim-pack Solar C18 reversed-phase column (5 µm, 250×4.60 mm) was used for the analysis. Differential scanning calorimetry (DSC) measurement was done in a Waters Discovery DSC25 instrument. Powder X-ray diffraction (PXRD) measurements were carried out in Bruker D8 Advance instrument. Room temperature (298 K) and low temperature (120 K) single crystal X-ray diffraction (SCXRD) experiments were performed in the Bruker D8 Quest and Bruker Smart Apex II Ultra instruments, respectively.

2. Computational details: The ground state (S_0) geometries of all molecules were optimized using density functional theory (DFT) and the excited state energies and geometries were calculated using time-dependent density functional theory (TDDFT) methods as implemented in QChem quantum chemistry package (version 6.0.2).[1] Ground state (S_0) optimization was performed using B3LYP[2] exchange-correlation functional and 6-31+g(d) basis set for all atoms. Solvent (Acetonitrile) effects were taken into account by polarized continuum model (PCM) using the integral equation formalism (IEFPCM).[3] The excited state calculations were done using CAM-B3LYP[4] exchange-correlation functional and 6-31+g(d) basis set. The first singlet (S_1) and triplet (T_1) excited state of all the systems were optimized at the TDDFT level where the triplets were

optimized within Tamm-Dancoff approximation (TDA)[5] to overcome the triplet instability issue. Natural Transition Orbitals (NTOs) were calculated by Singular Value Decomposition (SVD) of the transition density matrix.[6] Spin-orbit coupling matrix elements (SOCME) were calculated at different geometries considering one-electron part of the Breit-Pauli Hamiltonian.[7] Both NTOs and SOCME were calculated at the TDDFT level as implemented in QChem6 software. NTOs and absorption spectra were plotted using IQmol molecular visualization tool (version 3.1.2).[8]

3. Preparation of dopant-based guest@host solid solutions

Solvent evaporation method: To a solution of the host in chloroform taken in a round-bottom flask (50 mL), the guest (**DPB**) solution in chloroform was added, and the resulting mixture was concentrated on a rotary evaporator to get the bicomponent solid.

Melt casting method: A blend of two materials of the appropriate ratio was heated above the melting point of the higher melting component for 10 min under a nitrogen atmosphere and then rapidly cooled to room temperature to obtain the solid solution.

4. Friedel-Crafts acylation of biphenyl with oxalyl chloride

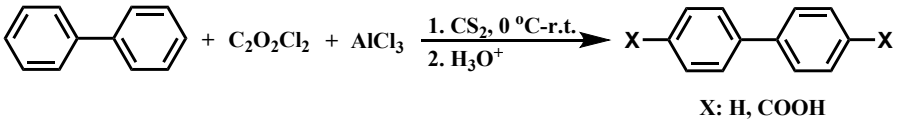

To biphenyl (1.0 g, 6.5 mmol, 1 equiv) taken in a round-bottom flask (250 mL), equipped with a magnetic stir bar, CS_2 was added (80 mL) and stirred to dissolve. Oxalyl chloride (1.8 mL, 21.0 mmol, 3.2 equiv) was added and the reaction mixture was cooled to 0 °C in an ice bath for 10 min. $AlCl_3$ (1.9 g, 14.2 mmol, 2.2 equiv) was added and the mixture was stirred for 1 h in N_2 atmosphere. More oxalyl chloride (1.8 mL, 21.0 mmol, 3.2 equiv) and $AlCl_3$ (1.9 g, 14.2 mmol, 2.2 equiv) were added sequentially and the reaction mixture was allowed to come to room temperature and continued overnight with constant stirring. Ice-cold water (150 mL) was added and stirred till a yellowish precipitate appeared. The volatile CS_2 was removed under reduced pressure. The precipitate was filtered, washed with HCl (0.5 M, 200 mL), water (200 mL) and dried to get yellowish solid (1.2 g). The crude product was orange emissive under a UV (365 nm) lamp. A part of the crude (500 mg) was column purified on silica gel (100-200 mesh size) using methanol-DCM (0–10 %), which yielded **FC-BCA** (266 mg) and a mixture of **FC-BCA** and **FC-BDCA** (see section 3A-2).

5. Esterification of FC-BCA (orange emissive material)

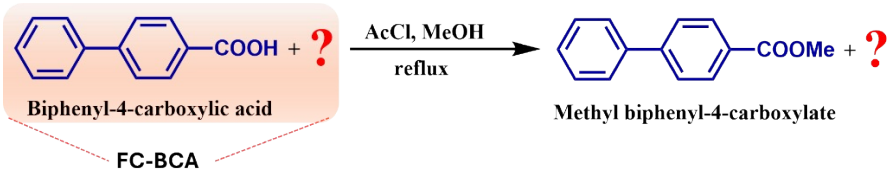

To MeOH (100 mL) taken in a round-bottom flask and cooled to 0 °C in an ice bath, equipped with a magnetic stir bar, AcCl (0.25 mL, 3.5 mmol, 4.6 equiv) was added and stirred for 10 min. **FC-BCA** (150 mg, 0.76 mmol, 1.0 equiv) was added and refluxed overnight in an argon atmosphere with constant stirring. The reaction mixture was concentrated, diluted with ethyl acetate (50 mL), washed with saturated $NaHCO_3$ (3×50 mL), water (1×50 mL), brine (1×50 mL), dried over anhydrous Na_2SO_4 and concentrated. The crude was purified by column chromatography on silica gel (100-200 mesh size) using DCM-hexane (30–80 %) to isolate the impurity (1.5 mg).

^{1}H NMR (400 MHz, $CDCl_3$) δ ppm: 8.15 (d, *J* = 8.4 Hz, 2H), 8.11 (d, *J* = 8.4 Hz, 2H), 8.08 (d, *J* = 8.8, 2H), 7.76 (dd, *J* = 9.2, 8.4 Hz, 4H), 7.70 (d, *J* = 8.4 Hz, 2H), 7.64 (d, *J* = 7.2 Hz, 2H), 7.49 (dd, *J* = 7.2, 7.6 Hz, 2H), 7.43 (t, *J* = 7.2 Hz, 1H) 3.96 (s, 3H).

HRMS: Calculated for $C_{28}H_{20}O_4Na$ [M+Na] 443.1259, Observed $C_{28}H_{20}O_4Na$ [M+Na] 443.1260.

6. Synthesis of diphenylbenzil (DPB)

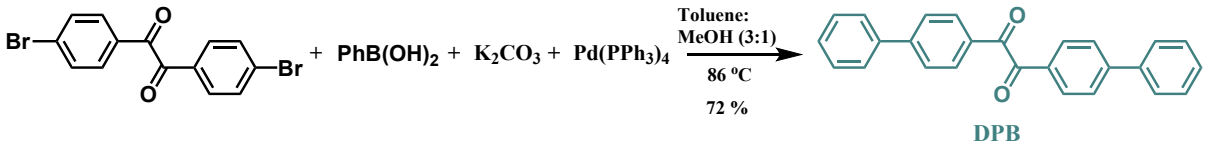

To a mixture of 4,4'-dibromobenzil (450 mg, 1.2 mmol, 1 equiv), phenylboronic acid (460 mg, 3.8 mmol, 3.1 equiv), tertrakis(triphenylphosphine)palladium(0) (71 mg, 0.06 mmol, 0.05 equiv) and potassium carbonate (1.1 g, 8.0 mmol, 6.5 equiv) taken in round-bottom flask (250 mL) equipped with a magnetic stir bar, a degassed mixture (120 mL) of toluene and methanol (3:1) was added and refluxed overnight in an argon atmosphere with constant stirring. The reaction mixture was concentrated on a rotary evaporator, dissolved in $CHCl_3$ (150 mL) and washed with brine (3×50 mL). The organic layer was dried over anhydrous Na_2SO_4 and concentrated to obtain the crude product, which was purified by column chromatography on silica gel (100-200 mesh size) using DCM-hexane (35–40 %) to get a pale green color solid **DPB** (320 mg, 72 %). The amorphous solid was recrystallized from hot MeOH-$CHCl_3$, resulting in pale green long needle-like crystals.

Melting point: 142-143 °C

^{1}H NMR (400 MHz, $CDCl_3$) δ ppm: 8.08 (d, *J* = 8.4 Hz, 4H), 7.75 (d, *J* = 8.4 Hz, 4H), 7.64 (d, 7.2 Hz, 4H), 7.49 (dd, J = 6.8, 8 Hz, 4H), 7.43 (t, J = 7.4, 2H). (Fig. 3A-51)

^{13}C NMR (100 MHz, $CDCl_3$) δ ppm:194.18, 147.69, 139.58, 131.80, 130.60, 129.11, 128.70, 127.73, 127.43. (Fig. 3A-52)

HRMS: Calculated for $C_{26}H_{18}O_2Na$ [M+Na] 385.1204, Observed $C_{26}H_{18}O_2Na$ [M+Na] 385.1205.

7. Synthetic scheme for BCA and BDCA by cross coupling reaction

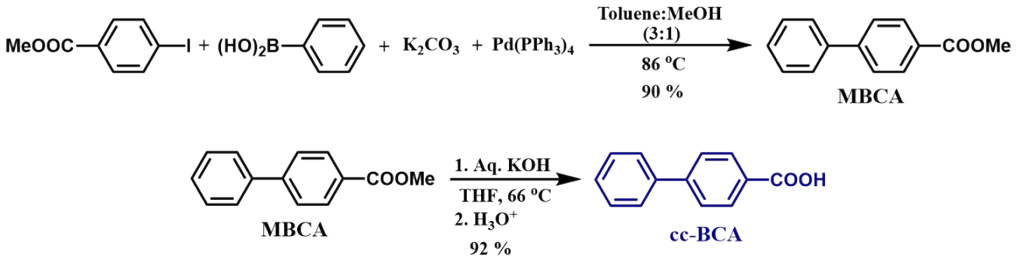

Scheme S1: Synthesis of **cc-BCA**.

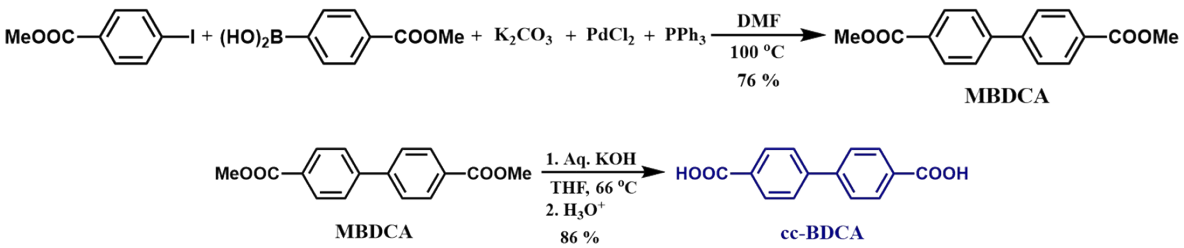

Scheme S2: Synthesis of **cc-BDCA**.

8. Synthesis of methyl 4-iodobenzoate

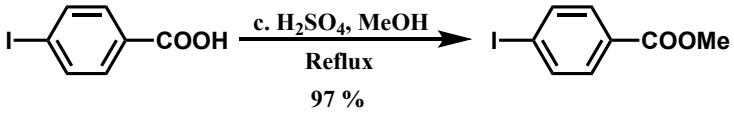

To a suspension of 4-iodobenzoic acid (2.0 g, 8.1 mmol, 1 equiv) in methanol (40 mL), concentrated H_2SO_4 (0.5 mL, 9.3 mmol, 1.2 equiv) was added and refluxed overnight with constant stirring. The reaction mixture was poured into ice-cold water (100 mL) and extracted with ethyl acetate (3×50 mL). The combined organic layer was washed with saturated $NaHCO_3$ solution (2×50 mL), water (1×50 mL), brine (1×100 mL), dried over anhydrous Na_2SO_4 and concentrated to obtain a pale orange solid which was passed through a silica plug to obtain white crystalline methyl 4-iodobenzoate (2.05 g, 97 %, melting point: 114–115 °C, lit.[9] 112-116 °C).

9. Synthesis of methyl biphenyl-4-carboxylate (MBCA)

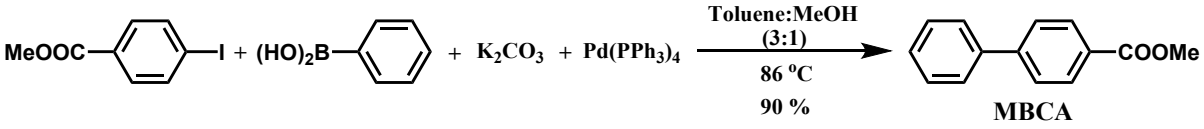

To a mixture of methyl 4-iodobenzoate (500 mg, 1.9 mmol, 1 equiv), phenylboronic acid (280 mg, 2.3 mmol, 1.2 equiv), tertrakis(triphenylphosphine)palladium(0) (100 mg, 0.086 mmol, 0.045 equiv) and potassium carbonate (650 mg, 4.7 mmol, 2.46 equiv) taken in a round-bottom flask (250 mL), equipped with a magnetic stir bar, a degassed mixture (120 mL) of toluene and methanol (3:1) was added and refluxed overnight in argon atmosphere with constant stirring. The reaction mixture was concentrated, dissolved in ethyl acetate (150 mL), washed with water (2×100 mL) and brine (2×100 mL). The organic layer was dried over anhydrous Na_2SO_4 and concentrated to obtain the crude product, which was purified by column chromatography on silica gel (100-200 mesh size) using ethyl acetate-hexane (2–2.5 %) to get a crystalline solid **MBCA** (365 mg, 90 %).

Melting point: 117–118 °C (lit.[10] 116-117 °C).

^{1}H NMR (400 MHz, $CDCl_3$) δ ppm: 8.11 (d, *J* = 8.8 Hz, 2H), 7.67-7.62 (m, 4H), 7.47 (dd, *J* = 8.4, 7.2 Hz, 2H), 7.39 (t, *J* = 7.4 Hz), 3.94 (s, 3H).

^{13}C NMR (100 MHz, $CDCl_3$) δ ppm:167.06, 145.68, 140.04, 130.14, 128.96, 128.92, 128.10, 127.32, 127.09, 52.18.

HRMS: Calculated for $C_{14}H_{13}O_2$ [M+H] 213.0916, Observed $C_{14}H_{13}O_2$ [M+H] 213.0920.

10. Synthesis of biphenyl-4-carboxylic acid (cc-BCA)

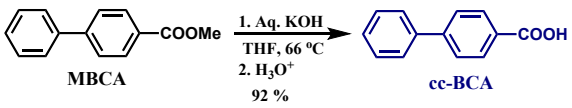

To **MBCA** (100 mg, 0.47 mmol, 1 equiv) dissolved in THF (7.5 mL), aqueous KOH (1 M, 2.5 mL, 2.5 mmol, 5.3 equiv) was added and refluxed for 6 h with constant stirring. THF was removed under reduced pressure, the reaction mixture was diluted with water (5 mL), acidified to pH 2 with 5 M aq. HCl. The white precipitate formed was filtered, washed with water (100 mL) and dried in a hot air oven, resulting in a white powdery solid **cc-BCA** (86 mg, 92 %).

^{1}H NMR (400 MHz, DMSO-D_6) δ ppm: 13.00 (s, 1H), 8.02 (d, *J* = 8.4 Hz, 2H), 7.80 (d, *J* = 8.4 Hz, 2H), 7.73 (d, *J* = 7.2 Hz, 2H), 7.50 (dd, *J* = 8, 7.2 Hz, 2H), 7.42 (t, *J* = 7.2 Hz, 1H), 2.08 (s, *acetone*).

^{13}C NMR (100 MHz, DMSO-D_6) δ ppm:167.14, 144.32, 139.09, 129.96, 129.61, 129.09, 128.30, 126.97, 126.82.

11. Synthesis of dimethyl biphenyl-4,4′-dicarboxylate (MBDCA)

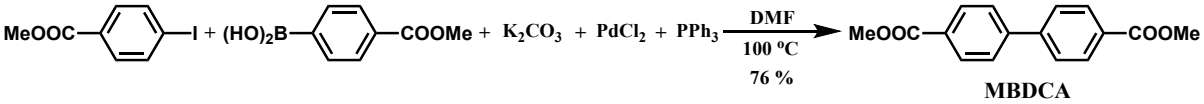

To a mixture of methyl 4-iodobenzoate (600 mg, 2.3 mmol, 1 equiv), 4-methoxycarbonylphenylboronic acid (412 mg, 2.3 mmol, 1.0 equiv), palladium(II) chloride (53 mg, 0.3 mmol, 0.13 equiv), PPh_3 (130 mg, 0.5 mmol, 0.22 equiv) and potassium carbonate (700 mg, 5.1 mmol, 2.2 equiv) taken in a round-bottom flask (250 mL) equipped with a magnetic stir bar, dry DMF (15 mL) was added and stirred overnight at 100 °C in an argon atmosphere. The cooled reaction mixture was diluted with brine (200 mL) and extracted with $CHCl_3$ (3×50 mL). The combined organic layer was washed with water (2×50 mL), brine (1×100 mL), dried over anhydrous Na_2SO_4 and concentrated to obtain the crude product, which was purified by column chromatography on silica gel (100-200 mesh size) using ethyl DCM-hexane (50–75 %) to get white solid **MBDCA** (472 mg, 76 %). The amorphous solid was recrystallized from hot ethyl acetate, resulting in colorless 2D sheet-like crystals.

Melting point: 214–216 °C (lit.[11] 213-215 °C).

^{1}H NMR (400 MHz, $CDCl_3$) δ ppm: 8.13 (d, *J* = 8.4 Hz, 4H), 7.69 (d, *J* = 8.8 Hz, 4H), 3.95 (s, 6H).

^{13}C NMR (100 MHz, $CDCl_3$) δ ppm:166.85, 144.40, 130.25, 129.74, 127.29, 52.28.

HRMS: Calculated for $C_{16}H_{15}O_4$ [M+H] 271.0970, Observed $C_{16}H_{15}O_4$ [M+H] 271.0968.

12. Synthesis of biphenyl-4,4′-dicarboxylic acid (cc-BDCA)

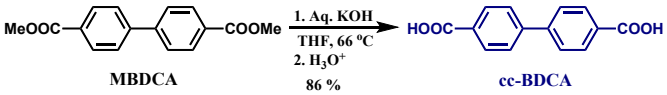

To **MBDCA** (295 mg, 1.1 mmol, 1 equiv) dissolved in THF (15 mL), aqueous KOH (1 M, 10 mL, 10.0 mmol, 9.1 equiv) was added and refluxed overnight with constant stirring. THF was removed under reduced pressure, the reaction mixture was diluted with water (10 mL) and acidified to pH 2 with 5 M aq. HCl. The white precipitate formed was filtered, washed with water (100 mL) and dried in a hot air oven, resulting in a white powdery solid **cc-BDCA** (230 mg, 86 %).

^{1}H NMR (400 MHz, DMSO-D_6) δ ppm: 8.04 (d, *J* = 8.4 Hz, 4H), 7.86 (d, *J* = 8.4 Hz, 4H).

^{13}C NMR (100 MHz, DMSO-D_6) δ ppm:167.19, 143.23, 130.48, 130.15, 127.28.

13. HPLC chromatogram of the polar fraction obtained during column purification of Friedel-Crafts reaction crude

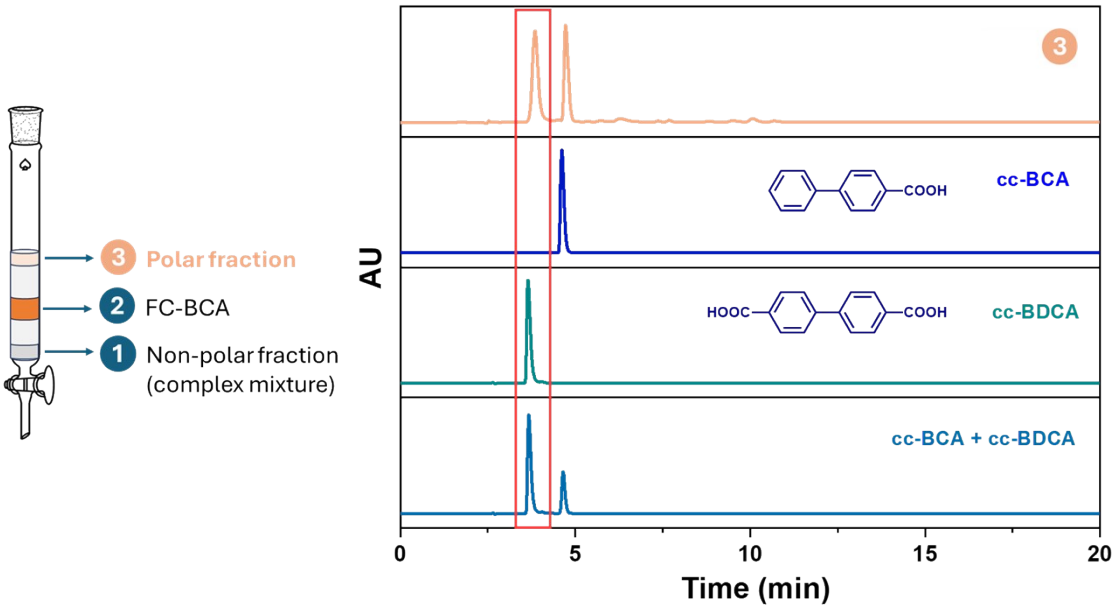

Fig. S1: HPLC chromatogram of the polar fraction (3) isolated from column purification of the reaction crude of Friedel-Crafts acylation of biphenyl with oxalyl chloride (section 3A.2.1), indicating the polar fraction is mixture of **BCA** and **BDCA**. (Solvent: 80% ACN-water with 0.2% AcOH)

14. Photoluminescence spectra of FC-BCA and lab synthesized BCA (cc-BCA)

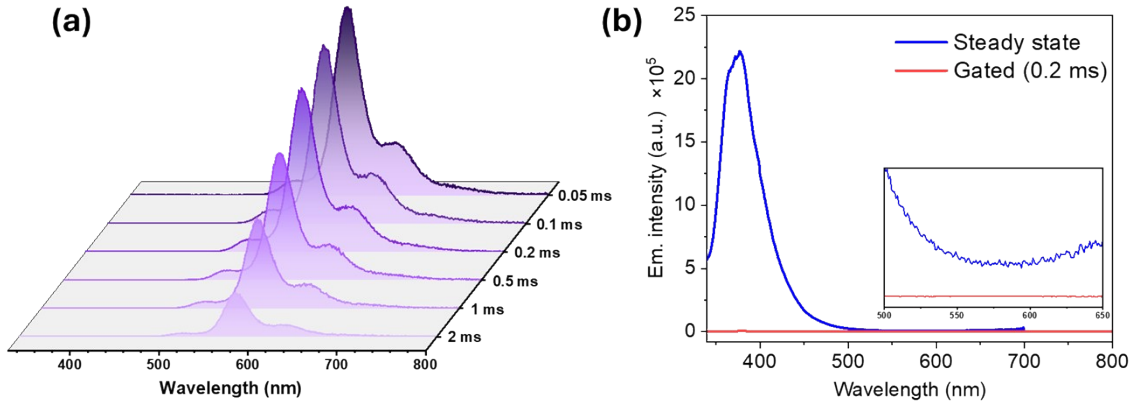

Fig. S2: (a) Gate time dependent photoluminescence spectra of **FC-BCA** (λ_{ex} 315 nm). (b) Lab synthesized **BCA** (**cc-BCA**) (inset: expanded spectrum in 500–650 nm range).

15. HPLC analysis of FC-BCA

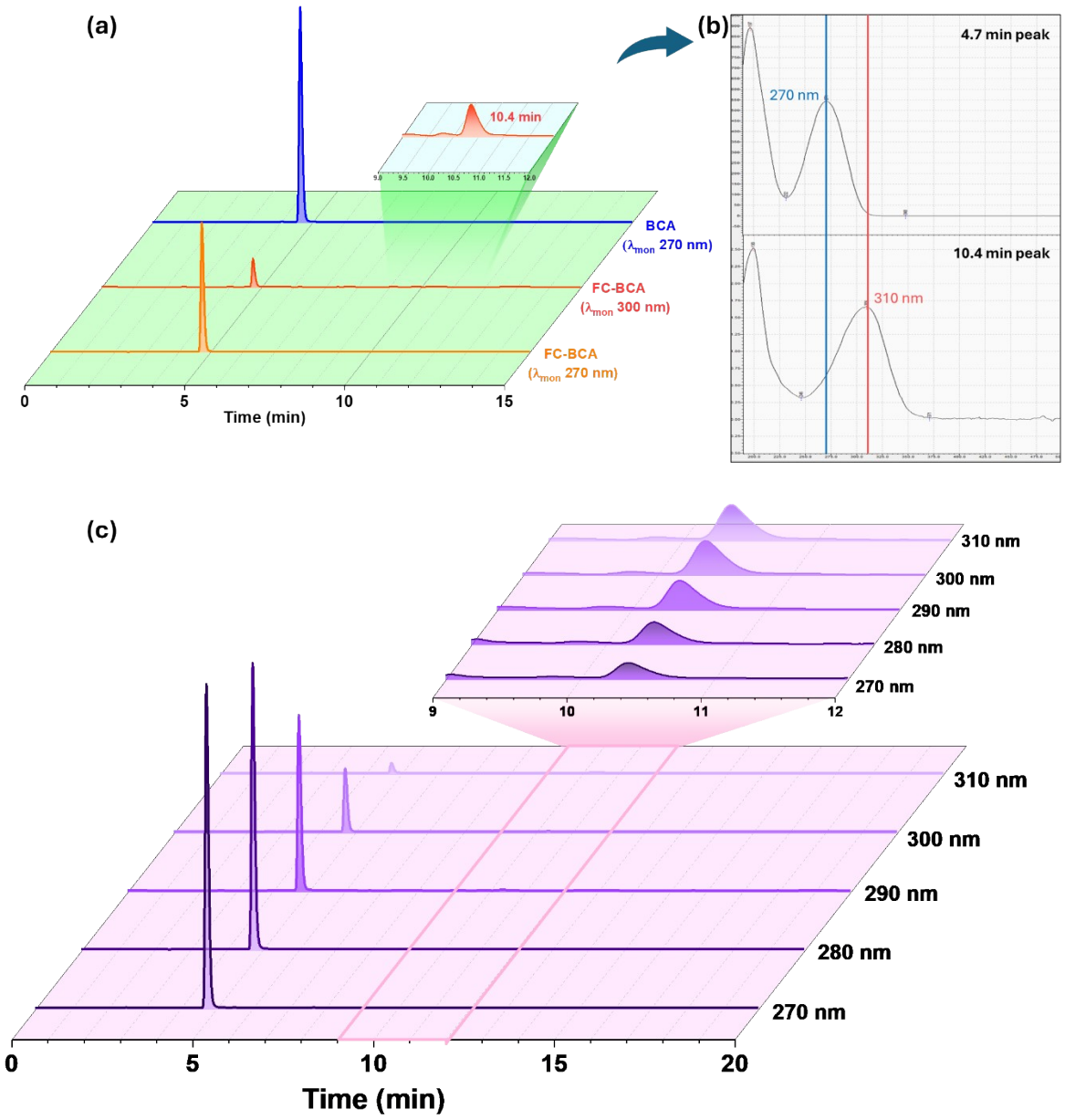

Fig. S3: (a) HPLC chromatogram of **FC-BCA** and pure **BCA** (inset: zoomed trace for **FC-BCA** monitored at 300 nm) (solvent: 80 % ACN-water with 0.2 % AcOH). (b) UV profile of 4.7 min and 10.4 min peaks appeared in the chromatogram of **FC-BCA**, generated by the PDA detector equipped with HPLC system. (c) HPLC trace of **FC-BCA** at different monitoring wavelengths.

16. Photoluminescence spectra of the solid solution prepared from BCA and HPLC concentrate

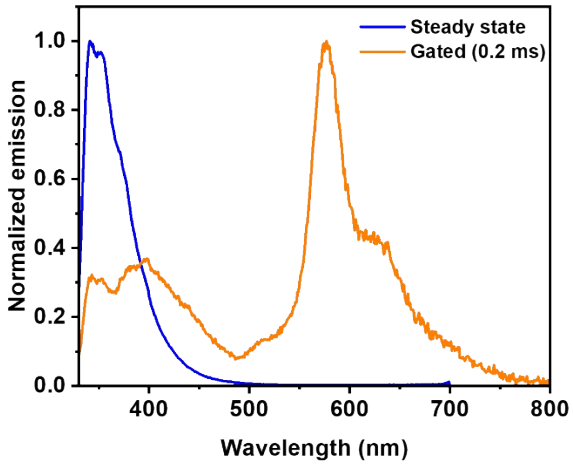

Fig. S4: Steady-state and gated (gate time: 0.2 ms) emission spectra (λ_{ex} 315 nm) of the bicomponent solid material prepared by solvent evaporation from a solution of pure **BCA** and HPLC concentrate of the 10.4 min peak collected from **FC-BCA**.

17. Supporting analytical data for DPB-COOMe

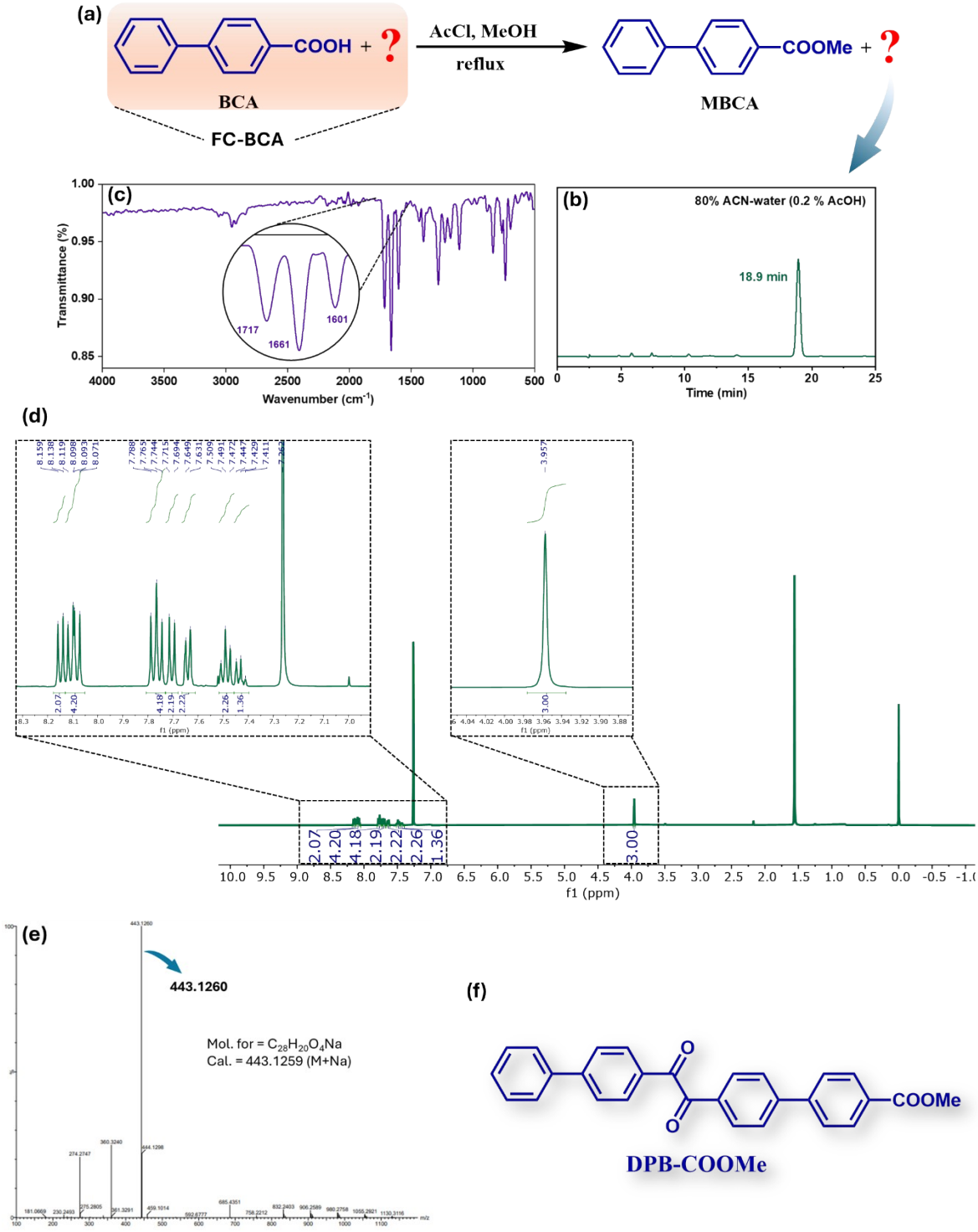

Fig. S5: (a) Synthetic scheme for the esterification of **FC-BCA**. (b) HPLC chromatogram of the isolated impurity monitored at 300 nm (solvent: 80 % ACN-water with 0.2 % AcOH). (c) FTIR spectrum, (d) ^{1}H NMR ($CDCl_3$, 400 MHz) spectrum (e) mass profile and (f) elucidated structure of the isolated impurity (**DPB-COOMe**).

18. Hydrolysis of DPB-COOMe

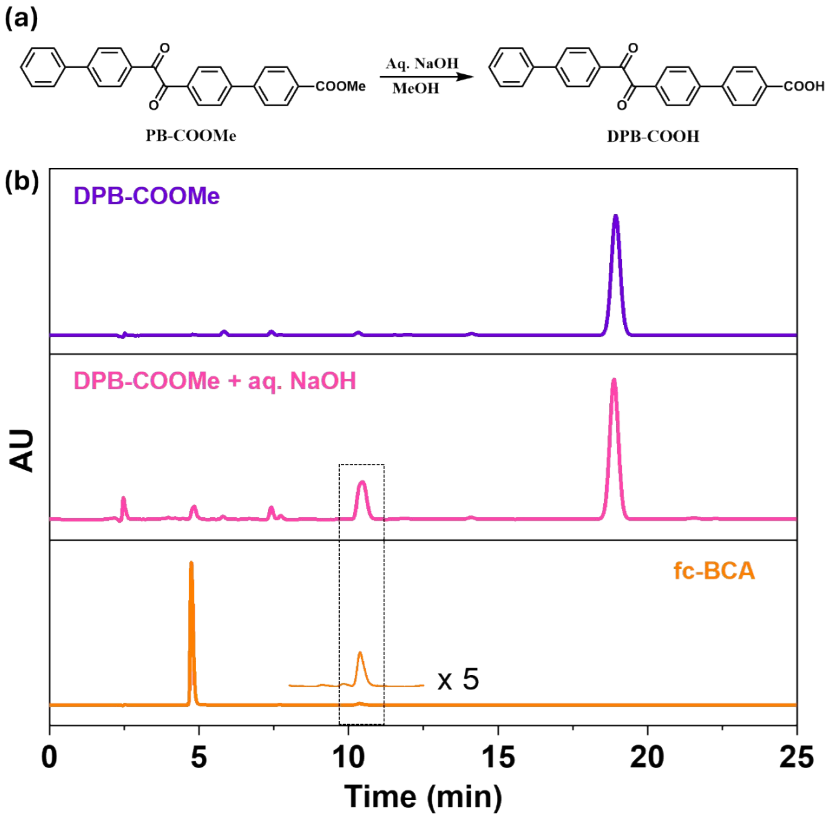

Fig. S6: (a) Scheme for the conversion of **DPB-COOMe** to **DPB-COOH**. (b) HPLC chromatogram of **DPB-COOMe**, acidified solution of **DPB-COOMe** treated with aq. NaOH and **FC-BCA** monitored at 300 nm (solvent: 80% ACN-water with 0.2 % AcOH).

19. HPLC of DPB

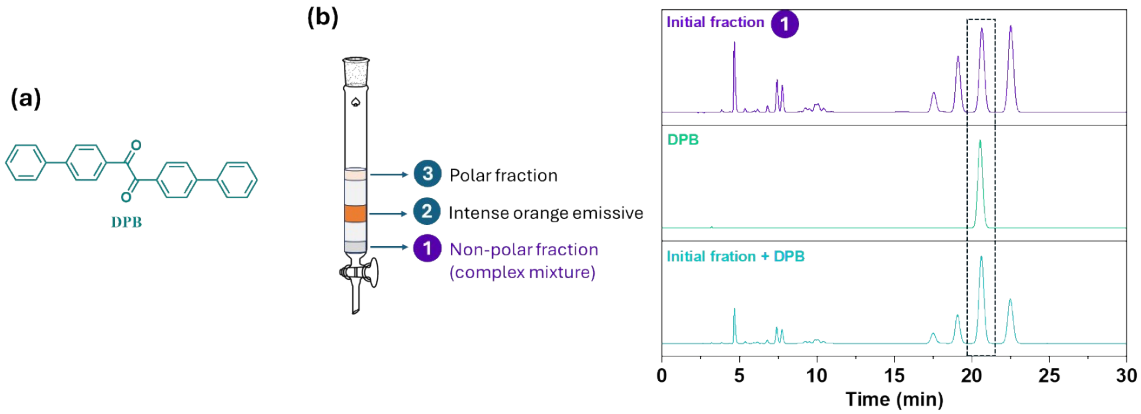

Fig. S7: (a) Structure of diphenylbenzil (DPB). (b) HPLC traces (λ_{mon} 300 nm) for the concentrated initial fraction (**1**, moved with the solvent front), **DPB** and **DPB** spiked **1** (Solvent: 80% ACN-water with 0.2 % AcOH).

20. Absorption and excitation spectra of DPB

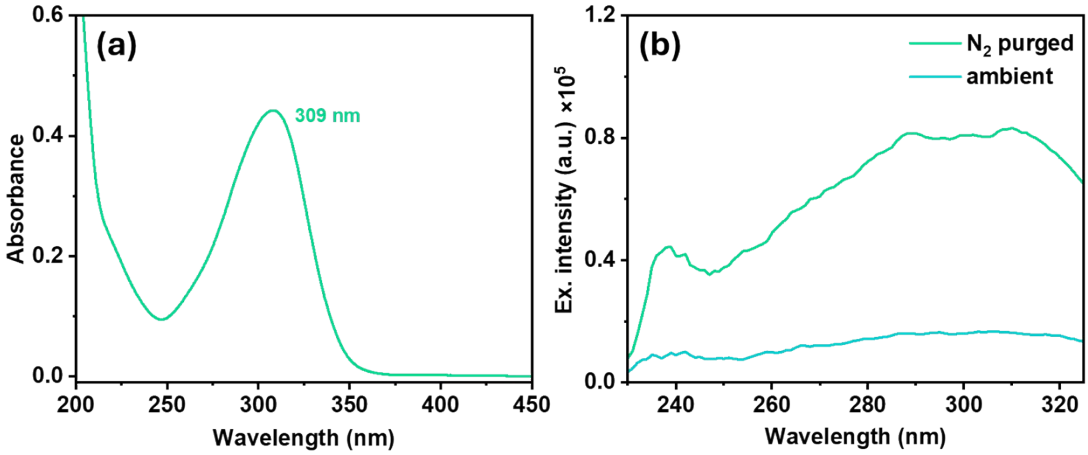

Fig. S8: (a) Absorption and (b) excitation (λ_{em} 560 nm) spectra of **DPB** (10 µM) in ACN.

21. Photoluminescent decay profile of DPB in solution at 77 K

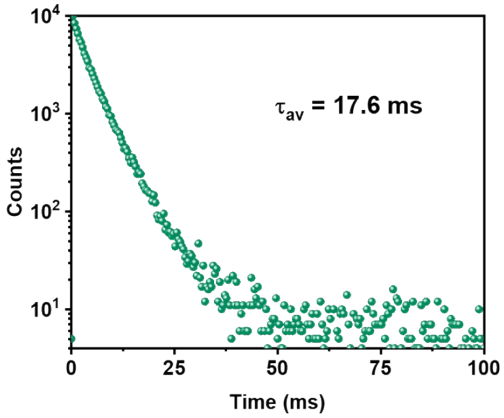

Fig. S9: Photoluminescence decay profile (λ_{ex} 310 nm, λ_{em} 545 nm) of **DPB** (10 µM) in ACN at 77 K.

22. Crystal parameters

Table S1: Crystal parameters of **DPB**

Parameters	298 K (CCDC 2427014)	120 K (CCDC 2427013)
Formula	$C_{26}H_{18}O_2$	$C_{26}H_{18}O_2$
Molar mass (g/mol)	362.4280	362.4280
Crystal system	Monoclinic	Monoclinic
Space group	C 2/c	C 2/c
a/Å	22.8524	22.76
b/Å	4.0599	3.955
c/Å	22.5935	22.51
α/°	90	90
β/°	118.082	117.86
γ/°	90	90
Cell volume/Å^3	1849.42	1791.4
Density (g/cm^3)	1.302	1.344
Z	8	8
Z’	1	1
R-Factor (%)	5.79	5.1
Wavelength/Å	0.71073	0.71073

23. Crystal packing of DPB

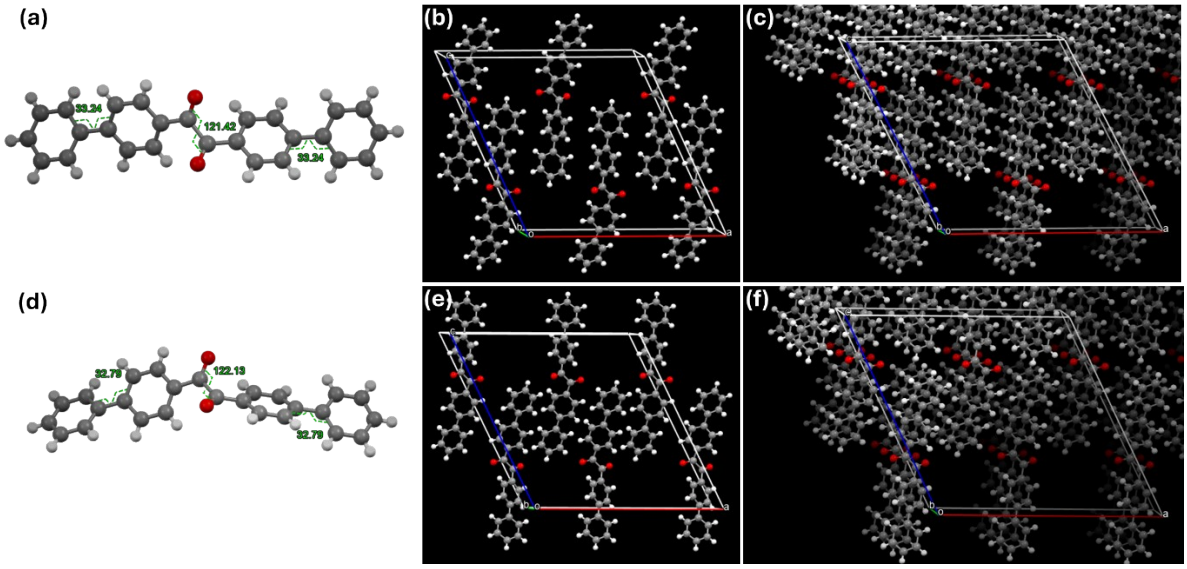

Fig. S10: (a) Crystal structure and (b), (c) molecular packing of **DPB** as obtained from SCXRD data recorded at 298 K (CCDC 2427014). (d) Crystal structure and (e), (f) molecular packing of **DPB** as obtained from SCXRD data recorded at 120 K (CCDC 2427013).

24. Hirsfeld surface analysis

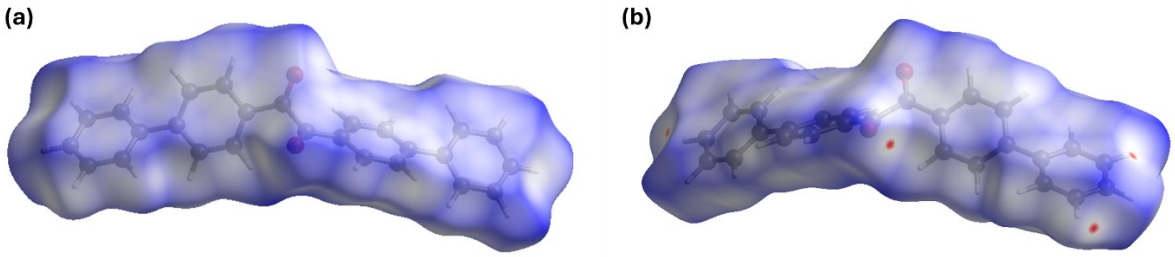

Fig. S11: Hirsfeld surface for **DPB** generated from SCXRD data obtained at (c) 298 and (d) 120 K. Hirsfeld surface was generated using CrystalExplorer[12] software. The surface is mapped with d_{norm} to visualize the extent of various intermolecular interactions. Simply, d_{norm} compares the distance of a point on the surface to the atoms interior and exterior of the surface to the sum of their van der Waals radii and generates a specific color contour— red, when the distance is smaller than the sum of their van der Waals radii, to white (distance is equal to the sum of their van der Waals radius) to blue for the distance larger than the sum of their van der Waals radii.

25. Natural transition orbitals for first excited triplet (T_1) state

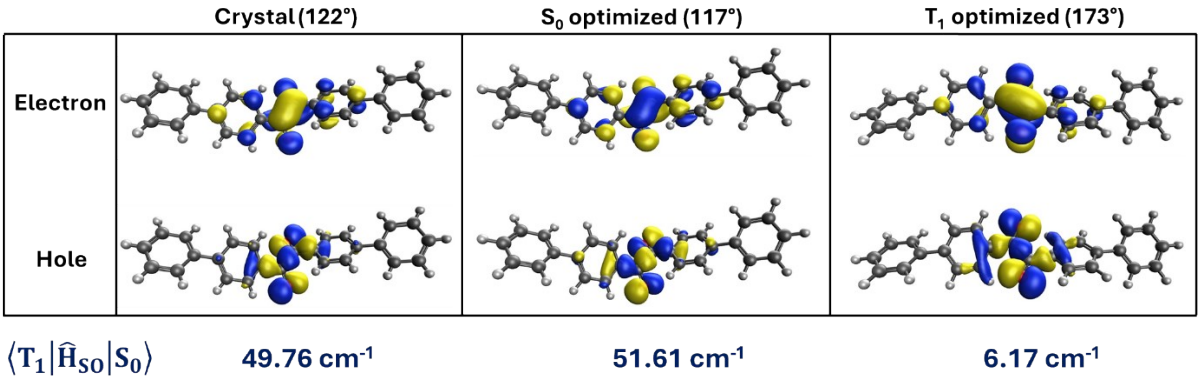

Fig. S12: NTOs for T_1 state in crystal (122°), S_0 (117°) and T_1 (173°) optimized geometries along with values of the respective SOCME with ground state (S_0) are mentioned below.

26. Oscillator strengths

Table S2: Oscillator strengths for $S_0 \rightarrow S_n$ transitions calculated at TDDFT level

Transition	**Oscillator strength**			
	S_0 opt. (117°)	**Crystal (122°)**	**Inter. geo. (143°)**	**T_1 opt. (173°)**
$S_0 \rightarrow S_1$	0.0011	0.0008	0.0003	0.11×10^{-5}
$S_0 \rightarrow S_2$	0.0209	-	-	-
$S_0 \rightarrow S_3$	1.2483	-	-	-
$S_0 \rightarrow S_4$	0.1809	-	-	-

27. Natural transition orbitals (NTOs) for $S_1/T_1/T_2$ states and excited state energies of DPB at different conformations

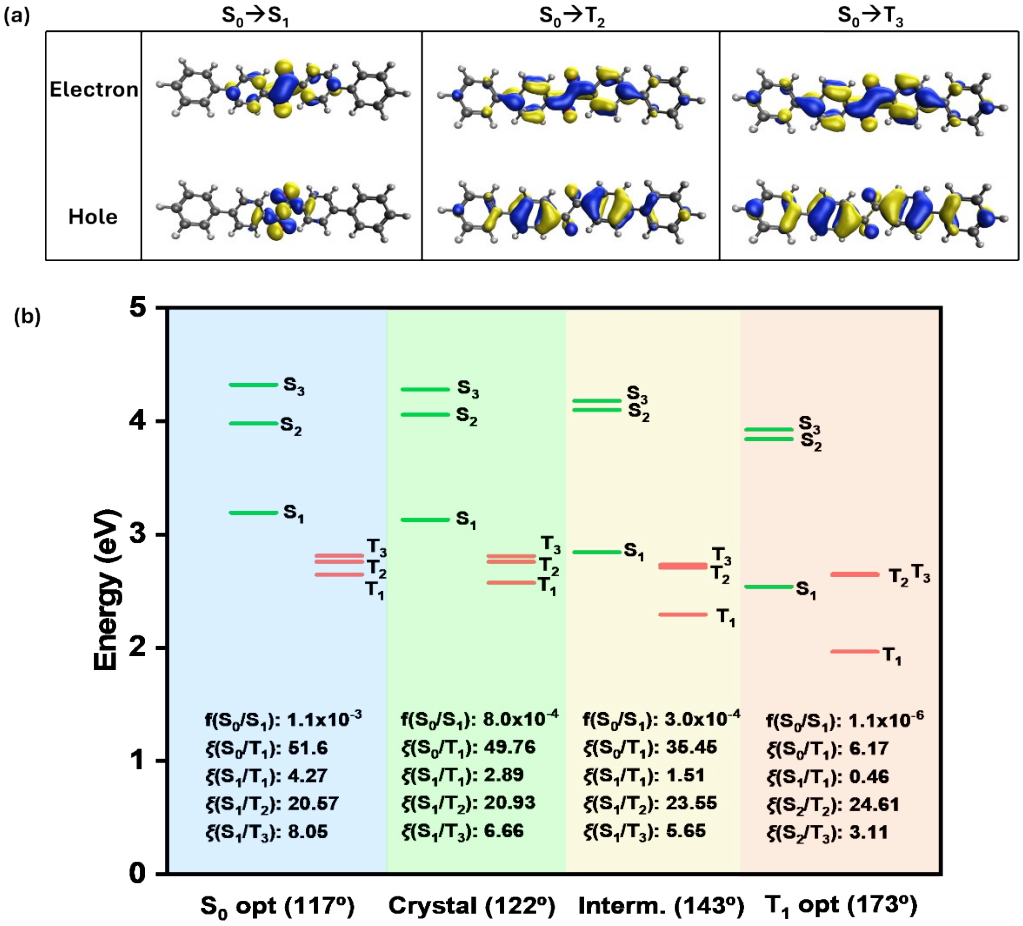

Fig. S13: (a) NTOs for $S_1/T_1/T_2$ states. (b) Simplified Jablonski diagram showing excited singlet (S_n) and triplet (T_n) state energies of **DPB** at different conformations, *i.e.*, at different dihedral angels between the carbonyls calculated at TDDFT level.

28. PXRD pattern of host and host/guest

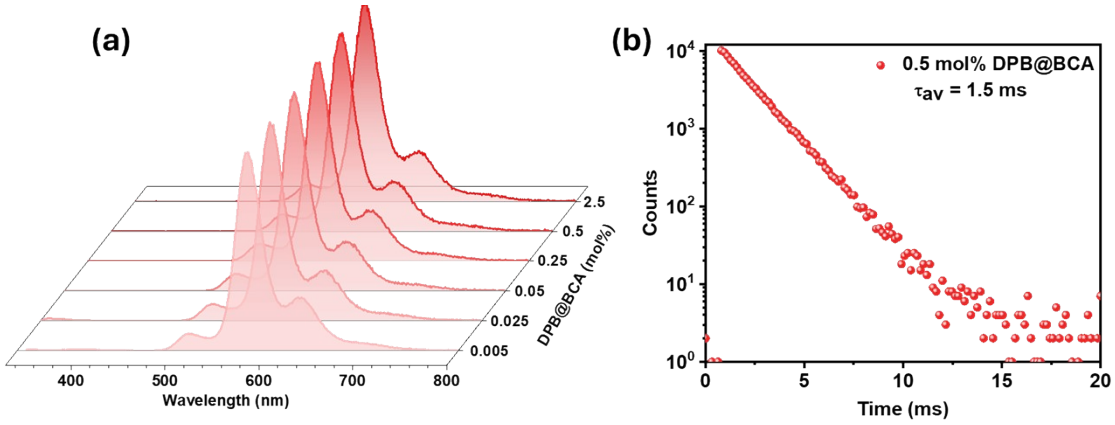

Fig. S14: (a) Gated (gate time: 0.2 ms) emission profile of **DPB@BCA**. (b) Photoluminescence decay profile (λ_{ex} 320 nm, λ_{em} 575 nm) of 0.5 mol% **DPB@BCA**.

29. Excitation and emission spectra of DPB@BCA

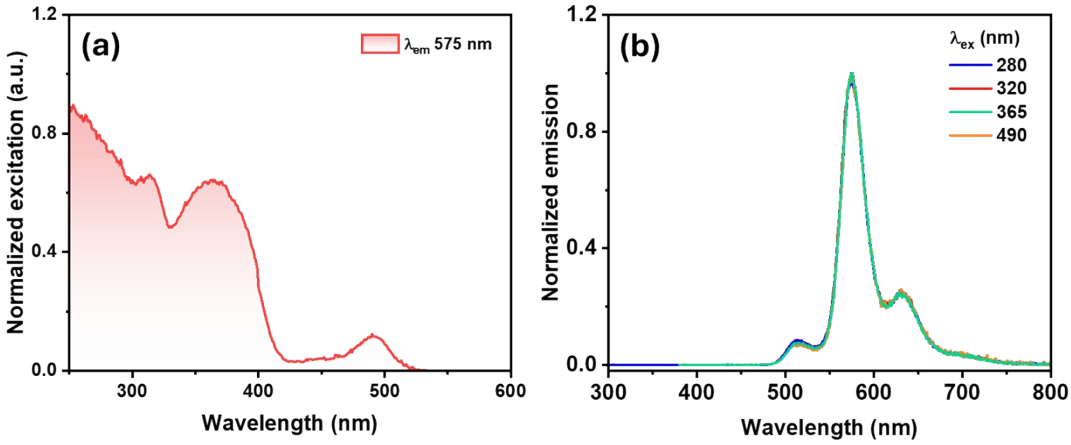

Fig. S15: (a) Excitation spectrum of 0.5 mol% **DPB@BCA** (λ_{em} 575 nm). (b) Gated (gate time: 0.2 ms) photoluminescence spectra of 0.5 mol% **DPB@BCA** at different λ_{ex}.

30. PXRD pattern of BCA and DPB@BCA

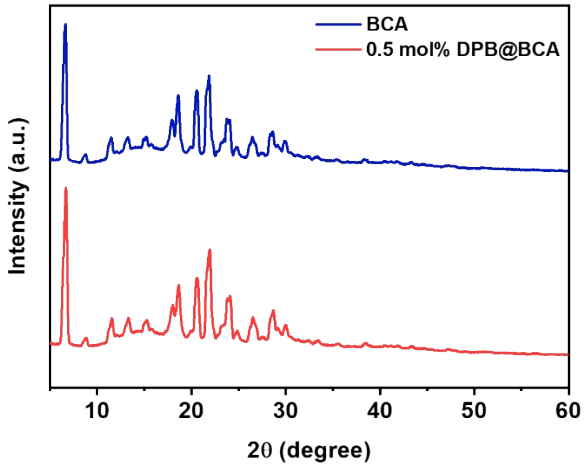

Fig. S16: Powder X-ray diffraction (PXRD) patterns of pristine and guest doped host **BCA**.

31. RTP lifetime of DPB@BCA

Table S3: RTP lifetime data of DPB@BCA at different dopant concentrations

DPB@BCA (mol %)	λ_{ex} (nm), λ_{em} (nm)	τ_1 (ms)	Relative contribution (%)	τ_{av} (ms)	χ^2
2.5	360, 515	1.36	100	1.36	0.993
	360, 575	1.37	100	1.37	1.187
	360, 630	1.36	100	1.36	0.993
	320, 515	1.34	100	1.34	1.501
	320, 575	1.35	100	1.35	1.131
	320, 630	1.34	100	1.34	1.163
	280, 515	1.43	100	1.43	1.266
	280, 575	1.45	100	1.45	0.996
	280, 630	1.44	100	1.44	1.064
0.5	360, 575	1.46	100	1.46	0.983
	320, 575	1.48	100	1.48	1.064
0.25	360, 575	1.47	100	1.47	1.045
	320, 575	1.50	100	1.50	1.034
0.05	360, 575	1.49	100	1.49	1.072
	320, 575	1.5	100	1.51	1.029
0.025	360, 575	1.49	100	1.49	1.107
	320, 575	1.56	100	1.56	1.227
0.005	360, 575	1.51	100	1.51	1.258
	320, 575	1.59	100	1.59	1.475

32. Phosphorescence decay profile of DPB@BCA

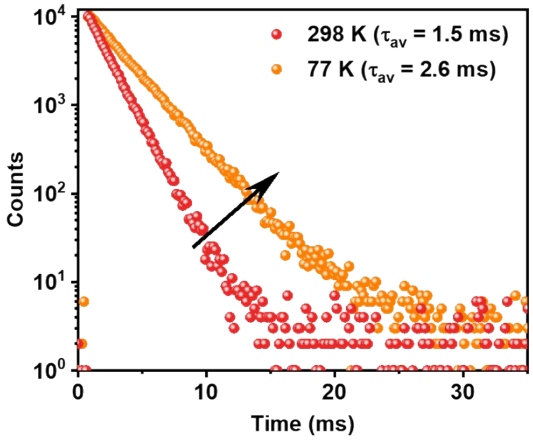

Fig. S17: Photoluminescence decay profile (λ_{ex} 360 nm, λ_{em} 575 nm) of 0.5 mol% **DPB@BCA** at 298 and 77 K.

33. Absorption and excitation spectra of BCA and DPB@BCA

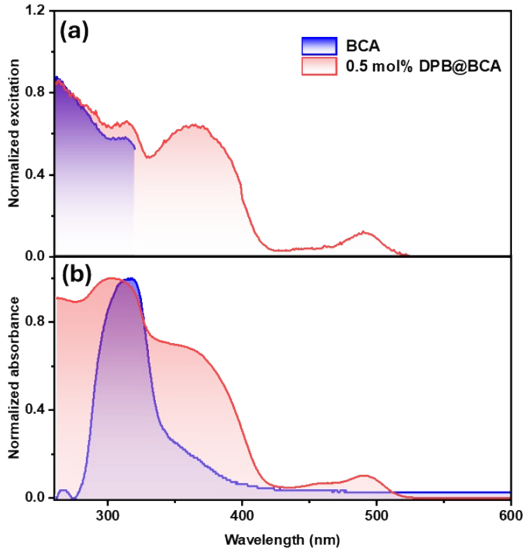

Fig. S18: (a) Excitation (λ_{em} 340 nm for **BCA**, λ_{em} 575 nm for **DPB@BCA**) and (b) absorption spectra of pristine and guest doped host.

34. Plausible triplet-to-triplet energy transfer (TTET) from BCA to DPB

To evaluate the feasibility of TTET from BCA to DPB, we calculated the singlet and triplet energies of **BCA**. As summarized in Table S4, both the S_1 and T_1 states of **BCA** are energetically higher than that of the **DPB**. **BCA** ensues intense blue-UV fluorescence and no discernible phosphorescence which can be attributed to finite oscillator strength for S_0-S_1 transition (0.6756) and very small SOCME for S_0/T_1 (1.38 cm^{-1}), respectively (Fig. S19). However, finite SOCME exists for S_1/T_n, implying an efficient intersystem crossing through any of the triplet states of **BCA** (Fig. S19). It would give rise to a significant population of T_1 state, which in turn can sensitize **DPB** in the solid host-guest matrix.

Table S4: Theoretically obtained excited state energies (eV) of **BCA** and **DPB**

States	S_1	S_2	S_3	S_4	T_1	T_2	T_3	T_4
BCA (32°)	4.75	4.92	4.97	5.19	2.96	3.71	4.27	4.45
DPB (117°)	3.19	3.98	4.32	4.56	2.65	2.76	2.81	3.48
DPB (173°)	2.54	3.84	3.92	3.93	1.96	2.64	2.65	3.32

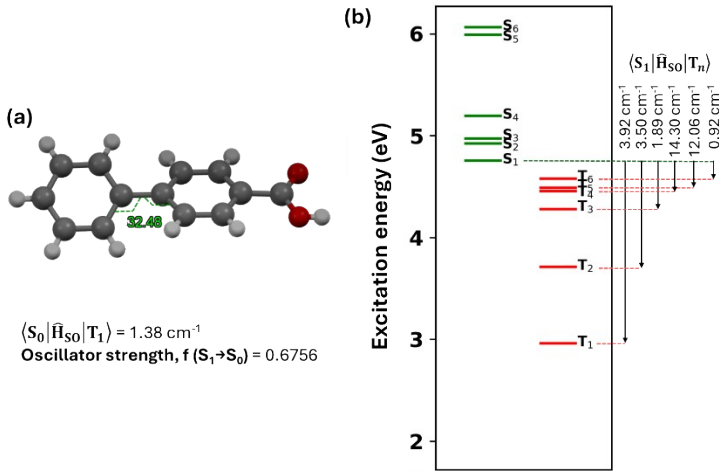

Fig. S19: (a) Crystal structure of **BCA** (obtained from CSD, CCDC code: 679622). (b) Excited singlet and triplet energies with SOCME (T_n/S_1) of **BCA** calculated at TDDFT level.

35. Fluorescence decay profile of host BCA

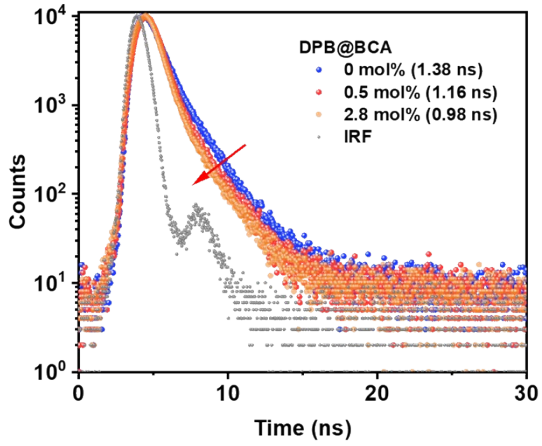

Fig. S20: (a) Luminescence decay profile of pristine, 0.5 mol% and 2.8 mol% **DPB** doped **BCA** (λ_{ex} 302 nm, laser; λ_{em} 340 nm).

36. Simulated absorption spectra of DPB

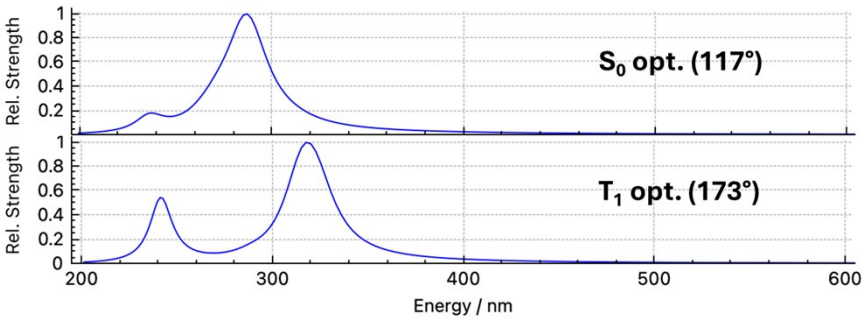

Fig. S21: Simulated absorption spectra (a plot of relative oscillator strength against wavelength, calculated using TDDFT) of **DPB** at S_0 (117°) and T_1 (173°) optimized geometries.

37. Formation of mixed state in DPB@BCA

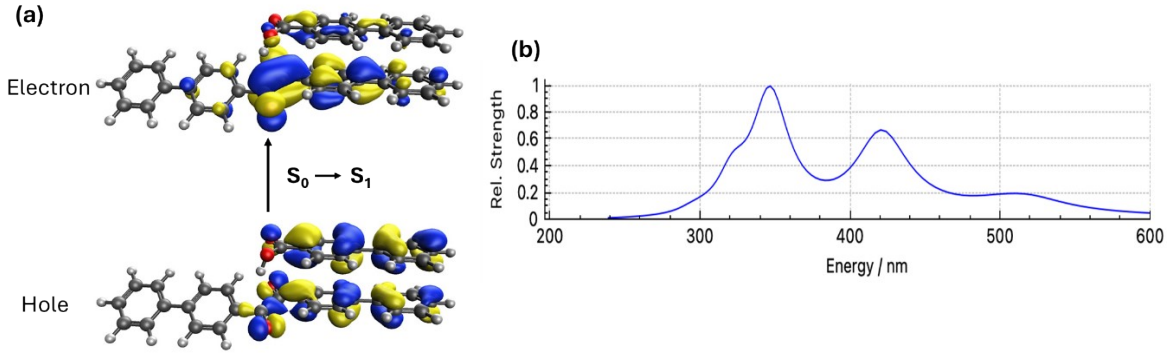

Fig. S22: (a) NTO ($S_0 \rightarrow S_1$) of **BCA** and **DPB** complex showing formation of a mixed state, comprised of charge transfer (CT) and local excitations (LE). (b) Simulated absorption spectra of **BCA** and **DPB** optimized complex, showing absorption band at 500 nm region.

38. PXRD pattern of host and host/guest

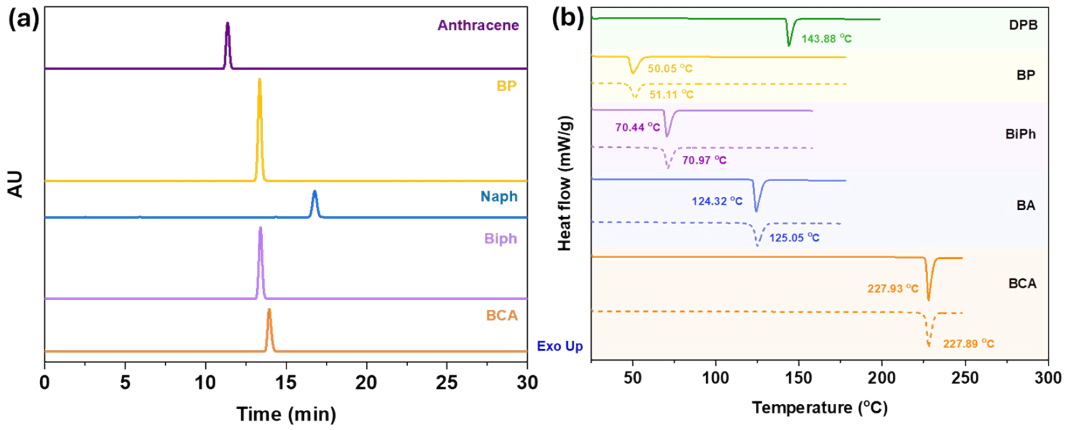

Fig. S23: (a) HPLC chromatogram of hosts: anthracene (80 % ACN-water), benzophenone (**BP**) (60% ACN-water), naphthalene (**NaPh**) (60%ACN-water), biphenyl (**BiPh**) (70% ACN-water), pure biphenyl-4-carboxylic acid (**BCA**) (50% ACN-water with 0.2% AcOH). (b) Differential scanning calorimetry (heating rate: 10 °C/min) traces of **DPB**, pristine host (solid line) and 0.5 mol% **DPB@host** (dotted line). Slight differences in the peak temperatures of pristine host and **DPB@host** suggest the formation of solid solutions (homogenous dispersion).

39. PXRD pattern of host and host/guest

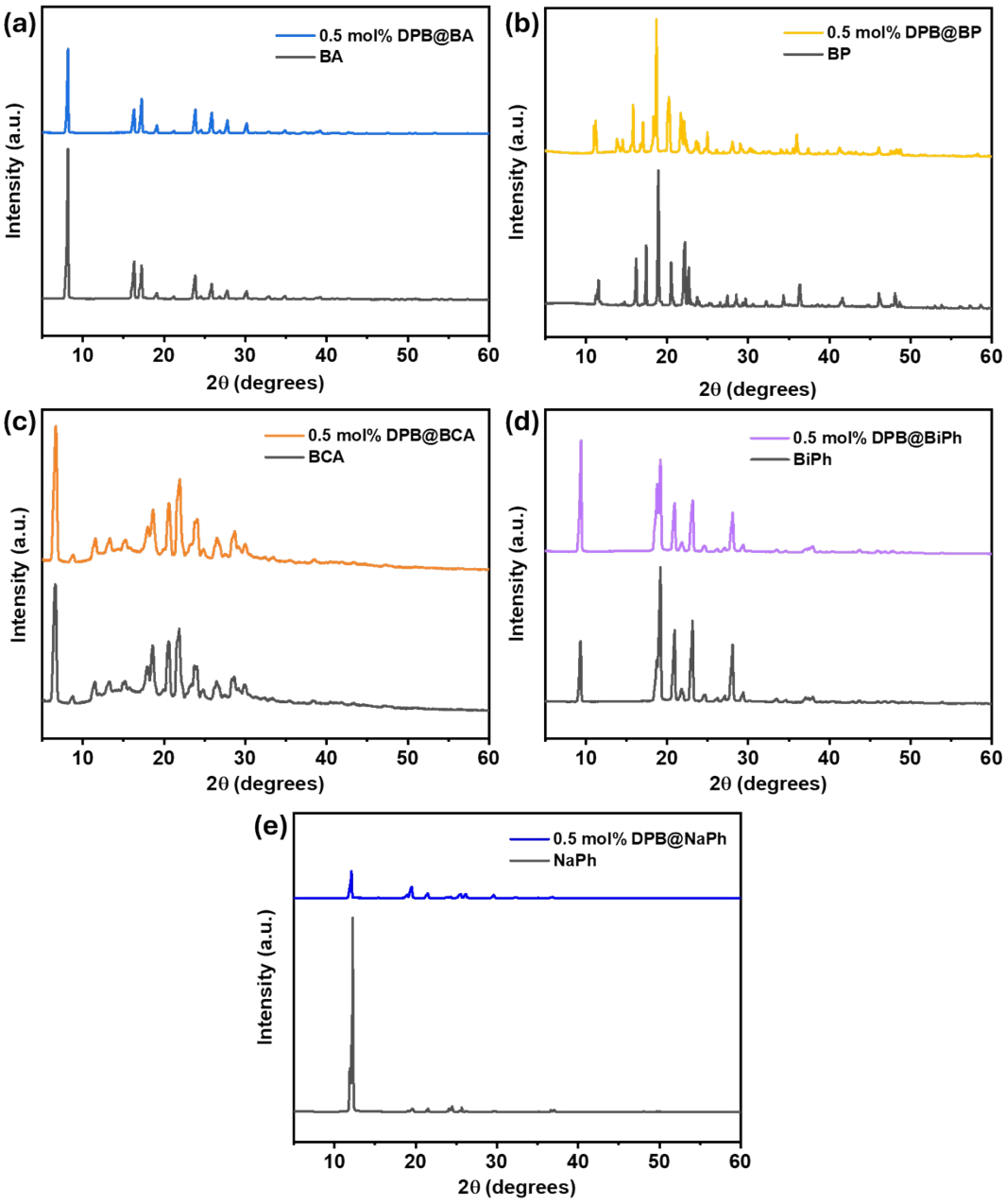

Fig. S24: PXRD pattern of pristine host and 0.5 mol% **DPB@host**. The similarity in pattern indicates that dopant (in such a low doping concentration) has no significant effect on host packing, ruling out the effect of crystal defects in RTP activation.

40. RTP lifetime and quantum yield data

Table S5: RTP lifetime data for 0.5 mol% **DPB@host** (298 K)

DPB@host	λ_{ex} (nm), λ_{em} (nm)	τ_1 (ms) (%)	τ_2 (ms) (%)	τ_3 (ms) (%)	τ_{av} (ms)	χ^2
Cryst DPB	410, 530	0.17 (72.45)	0.33 (27.55)		0.24	1.062
PMMA (1.0 wt%)	340, 535	0.05 (31.53)	0.21 (48.16)	0.80 (20.31)	0.54	1.342
BCA	360, 575	1.46 (100)			1.46	0.983
	490, 575	1.50 (100)			1.50	1.167
BiPh	365, 570	0.67 (100)			0.67	0.901
	485, 570	0.67 (100)			0.67	1.066
BA	345, 570	0.28 (9.12)	1.23 (90.88)		1.21	1.049
BP	380, 570	0.38 (92.77)	0.92 (7.23)		0.46	1.041
NaPh	365, 580	0.010 (0.78)*	0.90 (99.22)		0.90	1.086

*This component is possibly contributed by the guest molecules (**DPB**) on the surface of naphthalene that quickly undergo geometric relaxation post photoexcitation (see subsequent section, table S8).

Table S6: RTP quantum yield (Φ_{RTP}) of 0.5 mol% **DPB@host**

Host	λ_{ex} (nm)	Φ (%)
Cryst. Diphenylbenzil (DPB)	410	10.0
Biphenyl-4-carboxylic acid (BCA)	320	18.0
Biphenyl (BiPh)	365	26.4
Benzoic acid (BA)	345	22.8
Naphthalene (NaPh)	365	3.2
Benzophenone (BP)	380	4.5
PMMA (1 wt% DPB doped)	340	5.3

Table S7: Summary of the RTP properties of 0.5 mol% **DPB@host**

Host	**CIE-1931 coordinates (x, y)**	**τ_{av} (ms)**	**Φ (%)**
Cryst. Diphenylbenzil (DPB)	0.346, 0.612	0.24	10.0
Biphenyl-4-carboxylic acid (BCA)	0.504, 0.489	1.50	18.0
Biphenyl (BiPh)	0.488, 0.505	0.67	26.4
Benzoic acid (BA)	0.482, 0.509	1.21	22.8
Naphthalene (NaPh)	0.526, 0.468	0.90	3.2
Benzophenone (BP)	0.482, 0.504	0.46	4.5
PMMA (1 wt% DPB doped)	0.345, 0.594	0.54	5.3

41. Excitation/emission spectra of DPB@host and guest geometry prediction

We obtained the phosphorescence spectra at 77 K to understand the geometry of **DPB** embedded in different host matrices (Fig. S25). **DPB** embedded (0.5 mol%) in benzoic acid (**BA**) or benzophenone (**BP**) resulted in a green emission (λ_{em} 535 nm) at 77 K. As shown in Fig. S27b, c, e, and f, the phosphorescence profile is blue-shifted at cryogenic temperature which closely resembled the RTP of crystalline **DPB**. Therefore, **DPB** adopted the thermodynamically stable twisted conformation in **BA** and **BP** matrices. They provide a sufficient rigid environment to activate guest RTP, but not enough to restrict geometrical relaxation, resulting in distinct emissions at ambient (~575 nm) and cryogenic temperatures (~535 nm).

Interestingly, **DPB@BiPh** exhibited identical emission at 77 and 298 K, with the corresponding excitation profile extended up to 525 nm (Fig S25g to i). Clearly, the solid solutions in **BCA** and **BiPh** have similar optical features. Further, the TDDFT investigation indicated the presence of a mixed state (CT+LE) in the biphenyl-**DPB** one-to-one complex (not shown here). Therefore, biphenyl (**BiPh**) behaved like biphenyl-4-carboxylic acid (**BCA**), which may be attributed to the common biphenyl functionality in both hosts. Further, the single exponential decay of phosphorescence (table S5) proves the exclusivity of the linear conformation in **BiPh** (or **BCA**) as no other competitive excited state process is involved (like twisted conformer undergoing excited state geometry relaxation).

In contrast to **BA**, **BP**, **BiPh** (or **BCA**) that resulted in a distinct emission at 77 K, **DPB@NaPh**, particularly at lower guest doping (0.035 mol%), exhibited excitation-dependent dual emission at 77 K (Fig. S25m). When excited at 420 nm, emission at 530 nm dominated, whereas 365 nm excitation resulted in a structured emission centered at 580 nm, resembling RTP. We reasoned that the volatility of naphthalene exposed the surface **DPB** molecules that no longer experienced the matrix stabilization and eventually adopted a twisted conformation. On the other hand, **DPB** in the bulk host is stabilized in a linear geometry. The presence of two molecular species results in an excitation-dependent dual emission at 77 K— emission at 530 nm originating from the aggregated **DPB** molecules at the host surface, whereas **DPB** dispersed in the bulk host emitting at 580 nm. At room temperature, only one emission centered at 580 was observed as the surface exposed **DPB** molecules underwent geometric relaxation to a linear form post photoexcitation, which can be understood from a two-exponential fitting of the RTP decay profile. To prove our hypothesis, we freshly prepared bicomponent mixtures with two different guest concentrations, 0.035 mol% and 0.5 mol%, and compared their RTP decay profiles (table S8). The number of surface-exposed guest molecules is expected to be much higher in 0.5 mol% guest-embedded material, which may result in a different RTP decay pattern. As anticipated, freshly prepared 0.035 mol% and 0.5 mol% **DPB@NaPh** resulted in single and biexponential decay profiles, respectively (table S8). Moreover, the RTP lifetime of 0.035 mol% guest-embedded material recorded after a few months exhibited biexponential decay, with the RTP lifetime dropping from 1 ms to 0.8 ms, because the volatility of **NaPh** led to an increased number of surface-exposed guest molecules over time. Hence, it substantiates the presence of **DPB** in both twisted and linear conformations.

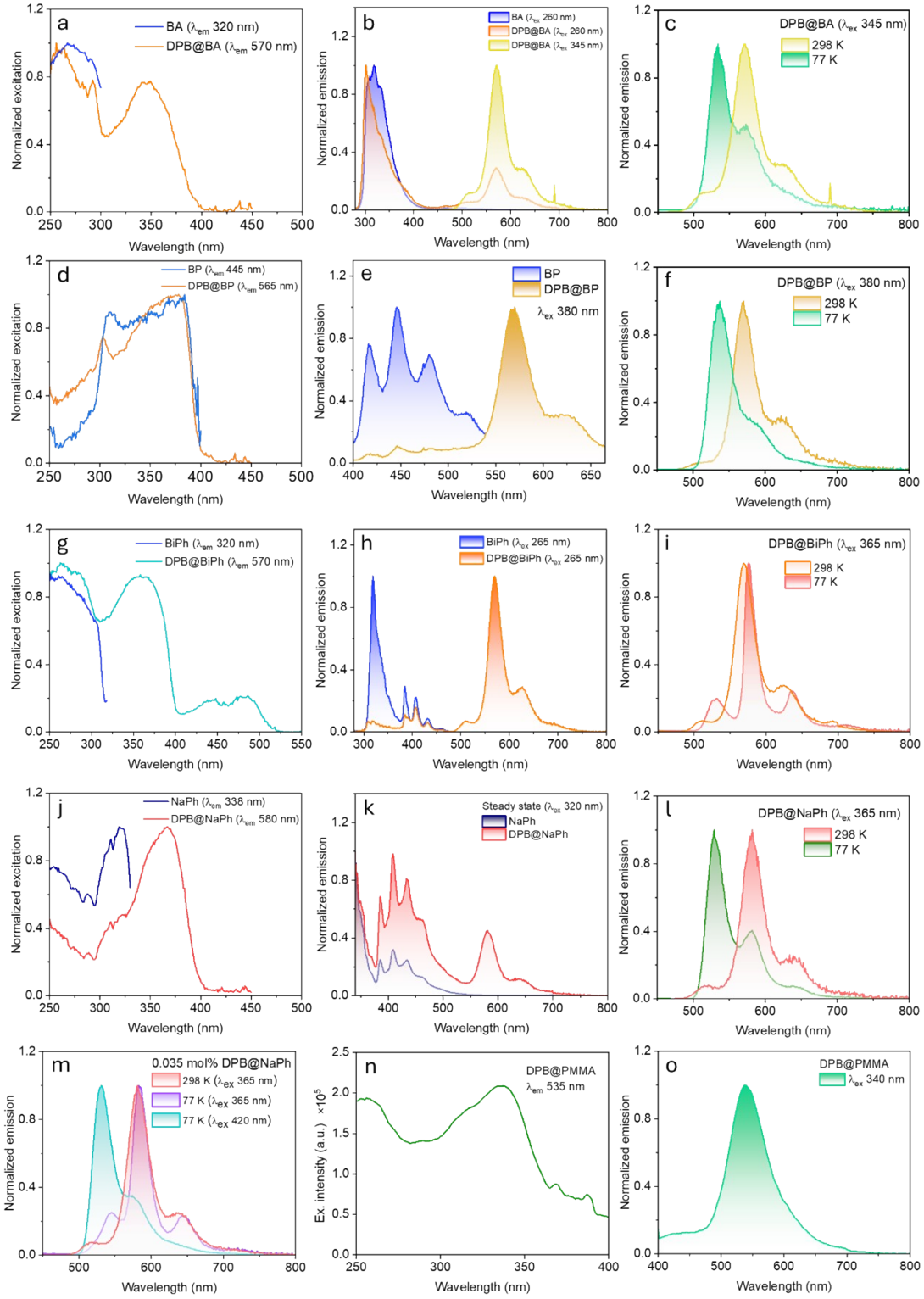

Fig. S25: Excitation and steady state photoluminescence spectra (at 298 K and 77 K) of pristine host and 0.5 mol% guest@host, (a), (b), (c) BA; (d), (e), (f) BP; (g), (h), (i) BiPh; (j), (k), (l) NaPh. (m) Steady state photoluminescence spectra of 0.035 mol% DPB@NaPh. (n) Excitation and (o) steady state photoluminescence spectra of 1 wt% DPB@PMMA at 298 K.

Table S8: RTP lifetime data for **DPB@NaPh** measured at room temperature (298 K)

DPB@NaPh (mol%)	**Sample description**	**λ_{ex} (nm), λ_{em} (nm)**	**τ_1 (ms) (%)**	**τ_2 (ms) (%)**	**τ_{av} (ms)**	**χ^2**
0.5 mol%	Freshly prepared	365, 580	0.010 (0.78)	0.90 (99.22)	0.90	1.086
	3 months old	365, 580	0.011 (7.14)	0.78 (92.86)	0.78	1.211
0.035 mol%	Freshly prepared	365, 580	0.99 (100)		0.99	1.045
	3 months old	365, 580	0.013 (2.20)	0.82 (97.80)	0.82	1.333

*The minor components resulted from the surface-exposed **DPB** molecules which undergo quick geometric relaxation post photoexcitation and barely ensue radiative emission at room temperature due to lack of sufficient matrix rigidification.

42. Emission spectra of guest@host for nonaromatic hosts

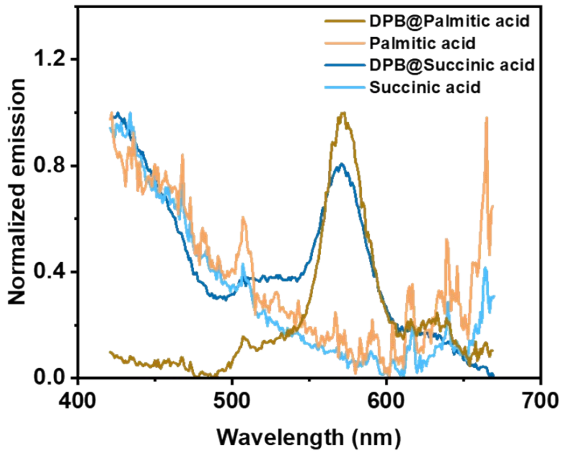

Fig. S26: Steady-state emission (λ_{ex} 350 nm) spectra of host and 0.5 mol% **DPB@host** at 298 K, host: palmitic acid and succinic acid.

43. Photoluminescence spectra and RTP decay profile of commercial BDCA

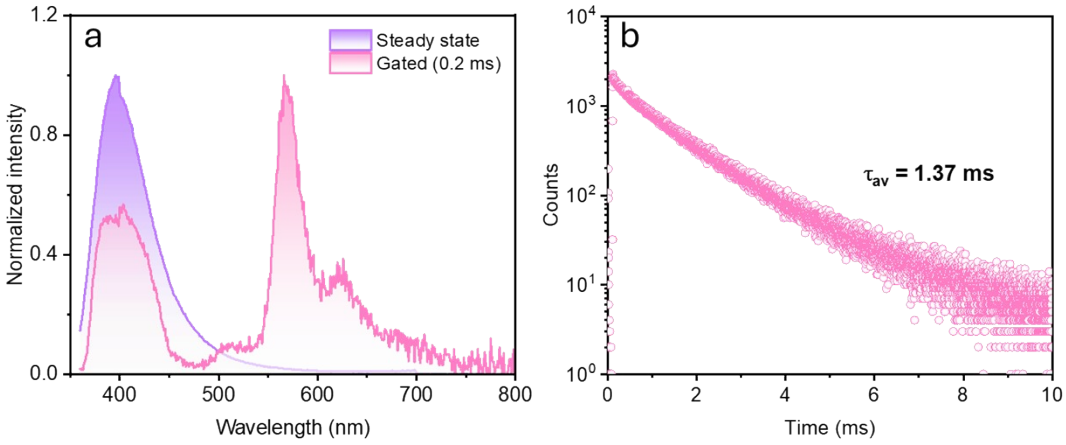

Fig. S27: (a) Photoluminescence spectra (λ_{ex} 340 nm) and (b) RTP decay profile (λ_{ex} 340 nm, λ_{em} 570 nm) of commercial **BDCA** (Fluka).

44. RTP lifetime data for com/cc-BDCA

Table S9: RTP lifetime data for **com/cc-BDCA** (298 K)

Sample	**λ_{ex} (nm), λ_{em} (nm)**	**τ_1 (ms) (%)**	**τ_2 (ms) (%)**	**τ_{av} (ms)**	**χ^2**
Aldrich*	340, 570	0.50 (19.55)	1.34 (80.45)	1.27	1.236
Fluka*	340, 570	0.51 (18.36)	1.44 (81.64)	1.37	1.241
0.1 mol% DPB@cc-BDCA	340, 570	1.26 (100)		1.26	1.202

*Since RTP from the commercial samples was weak, the luminescence decay was recorded in a gated mode (0.1 ms) to minimize interference from the prompt fluorescence of **BDCA**.

45. HPLC traces of commercial and lab synthesized BDCA

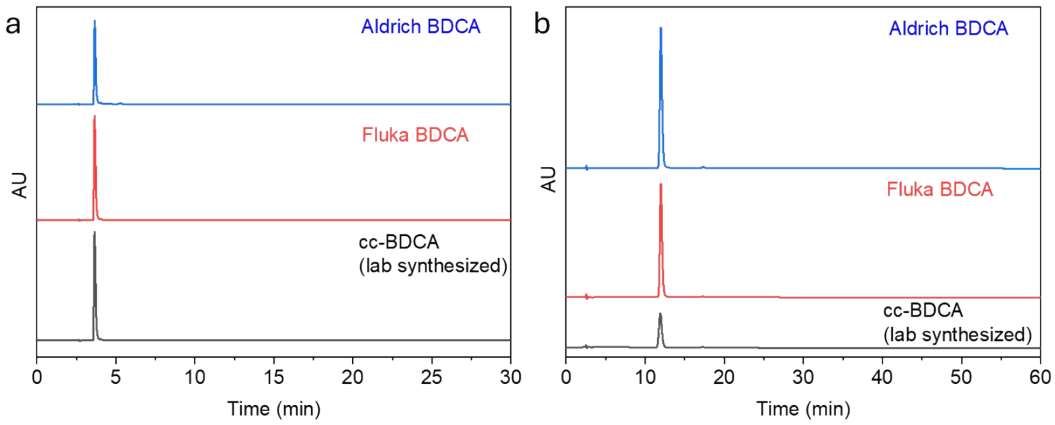

Fig. S28: HPLC chromatogram of commercial (sourced from Aldrich and Fluka) and lab synthesized **BDCA** (**cc-BDCA**): (a) 80% ACN-water with 0.2% AcOH and (b) 35% ACN-water with 0.2% AcOH.

46. Photoluminescence spectra of crystallized commercial BDCA

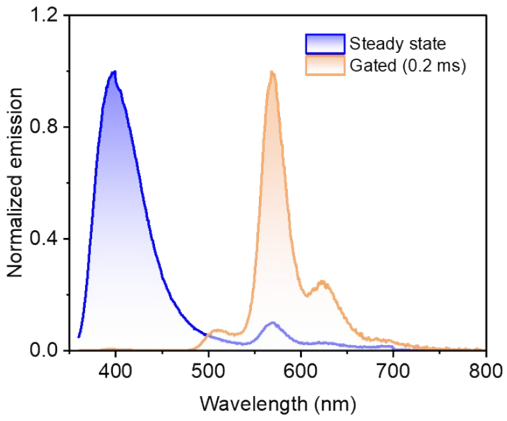

Fig. S29: Photoluminescence spectra (λ_{ex} 340 nm) of crystallized **com-BDCA**.

47. NMR spectra

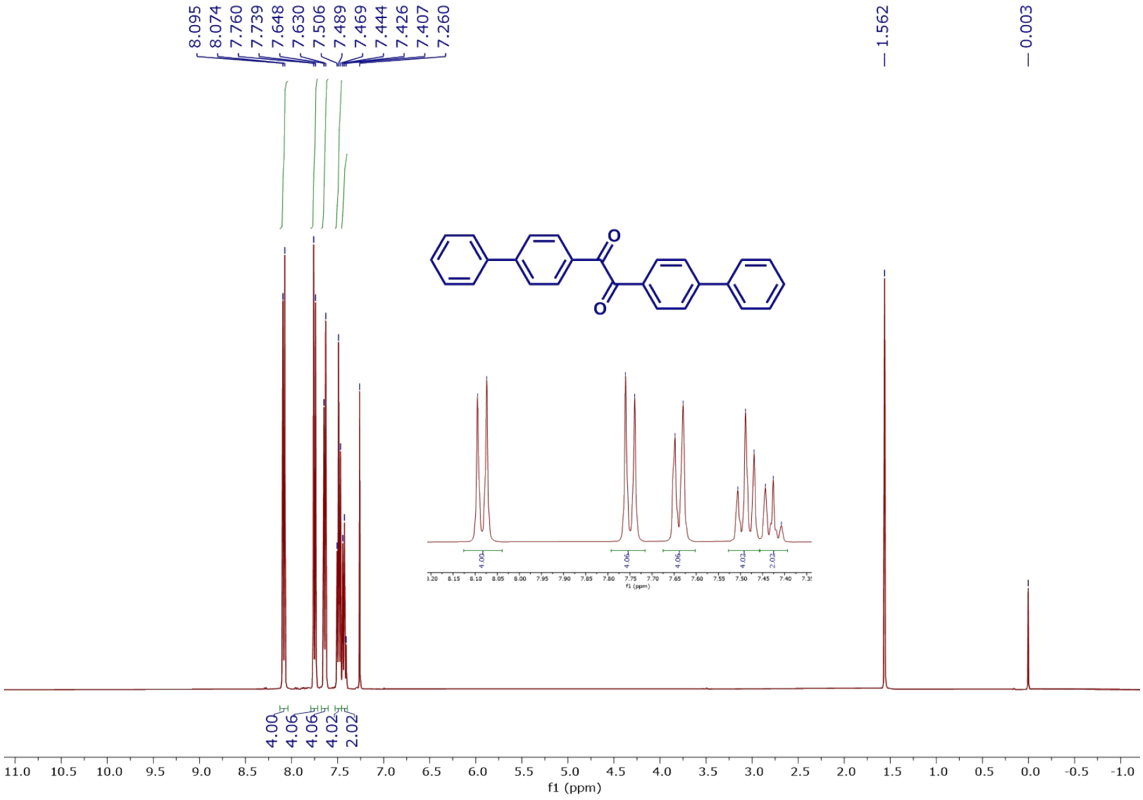

Fig. S30: ^{1}H NMR spectrum of diphenylbenzil (**DPB**) ($CDCl_3$, 400 MHz).

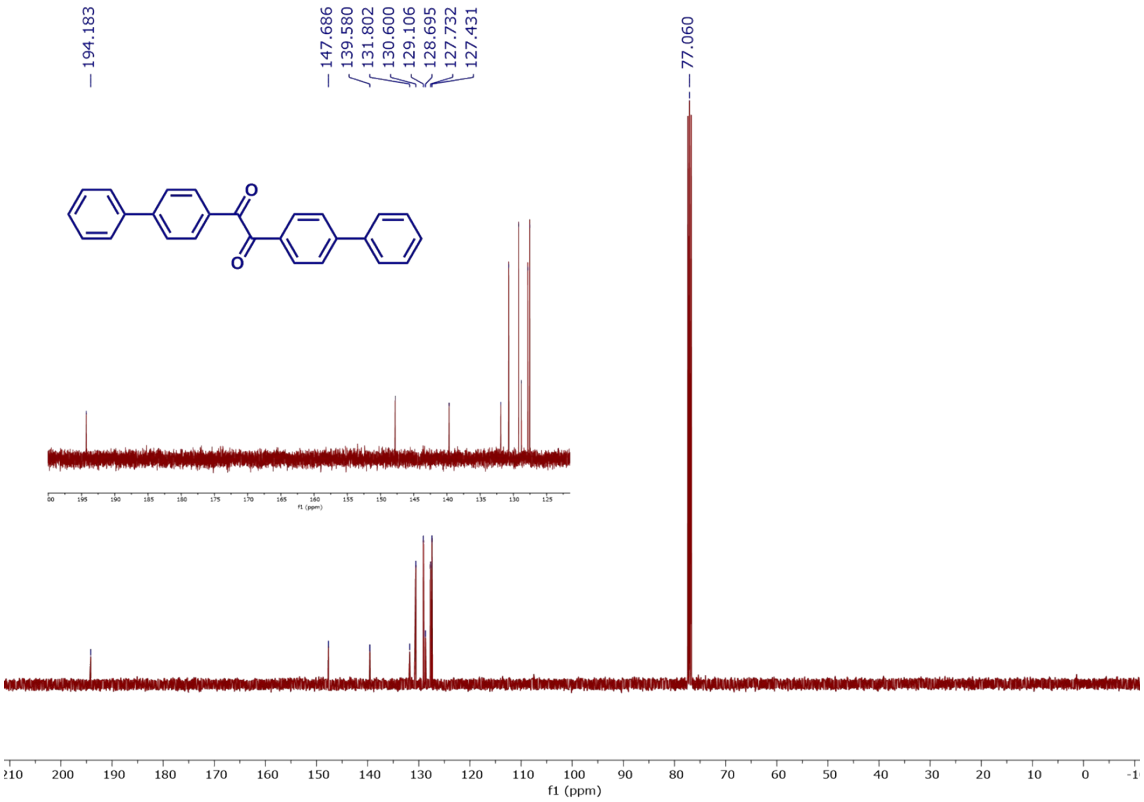

Fig. S31: ^{13}C NMR spectrum of diphenylbenzil (**DPB**) ($CDCl_3$, 100 MHz).

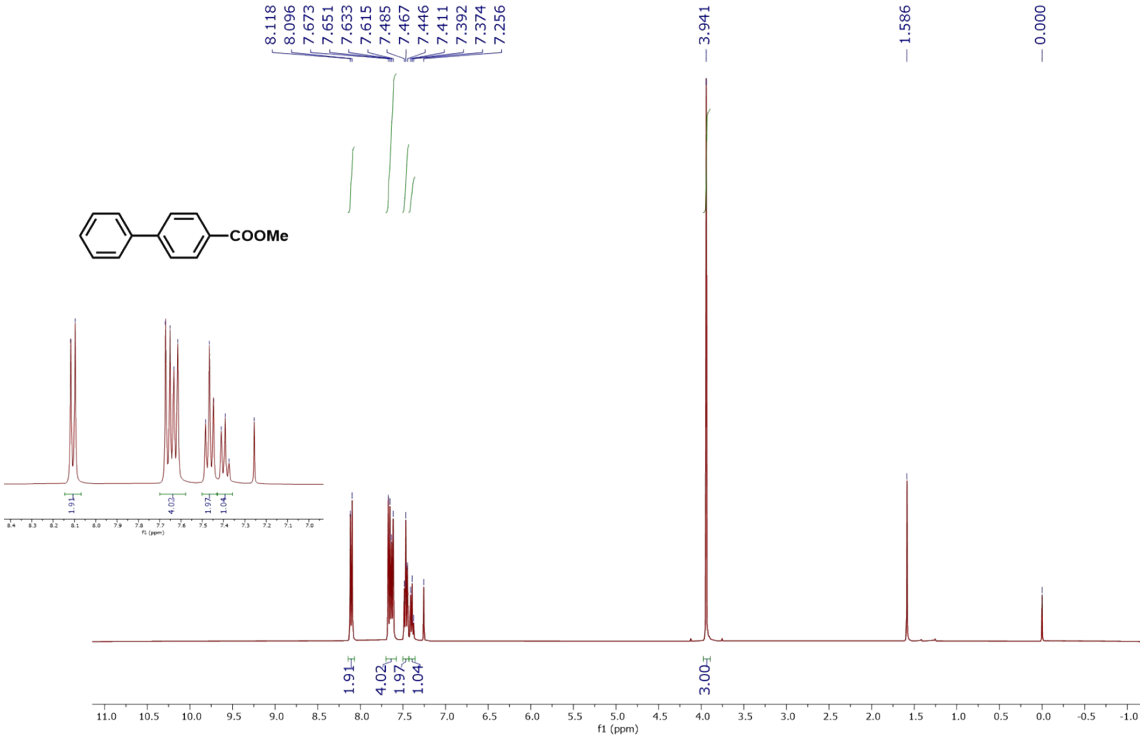

Fig. S32: ^{1}H NMR spectrum of methyl biphenyl-4-carboxylate (**MBCA**) ($CDCl_3$, 400 MHz).

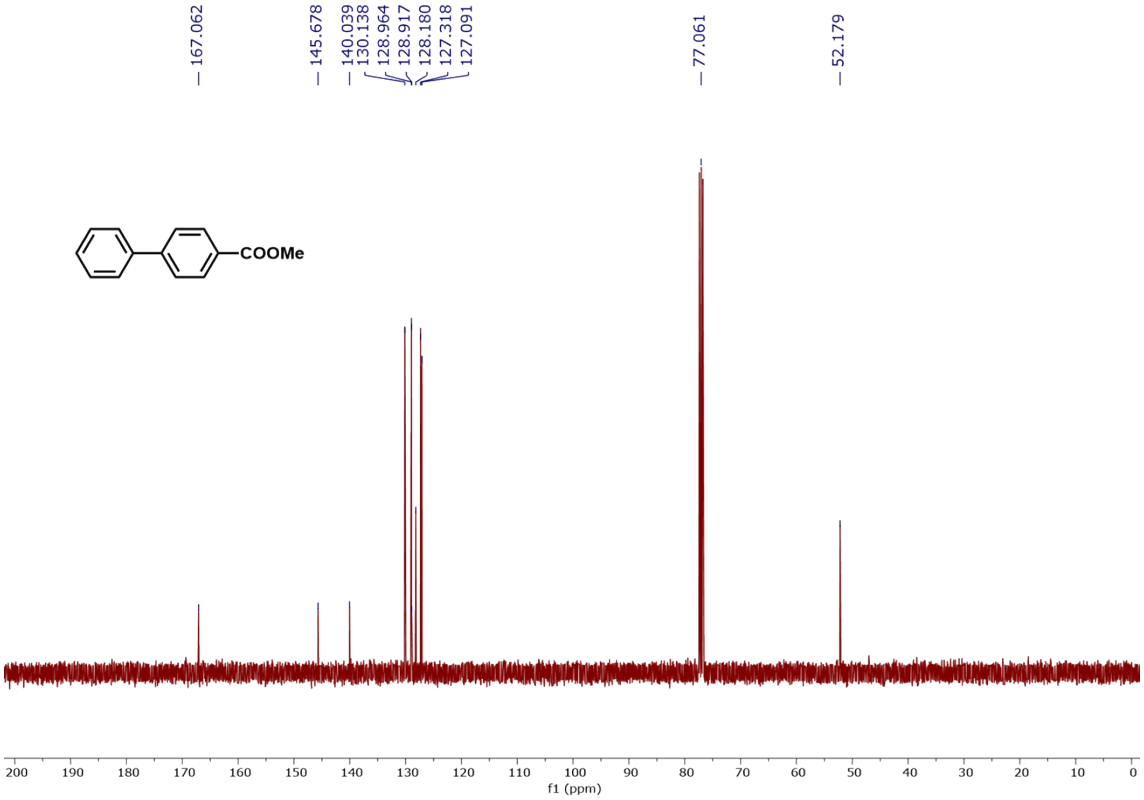

Fig. S33: ^{13}C NMR spectrum of methyl biphenyl-4-carboxylate (**MBCA**) ($CDCl_3$, 100 MHz).

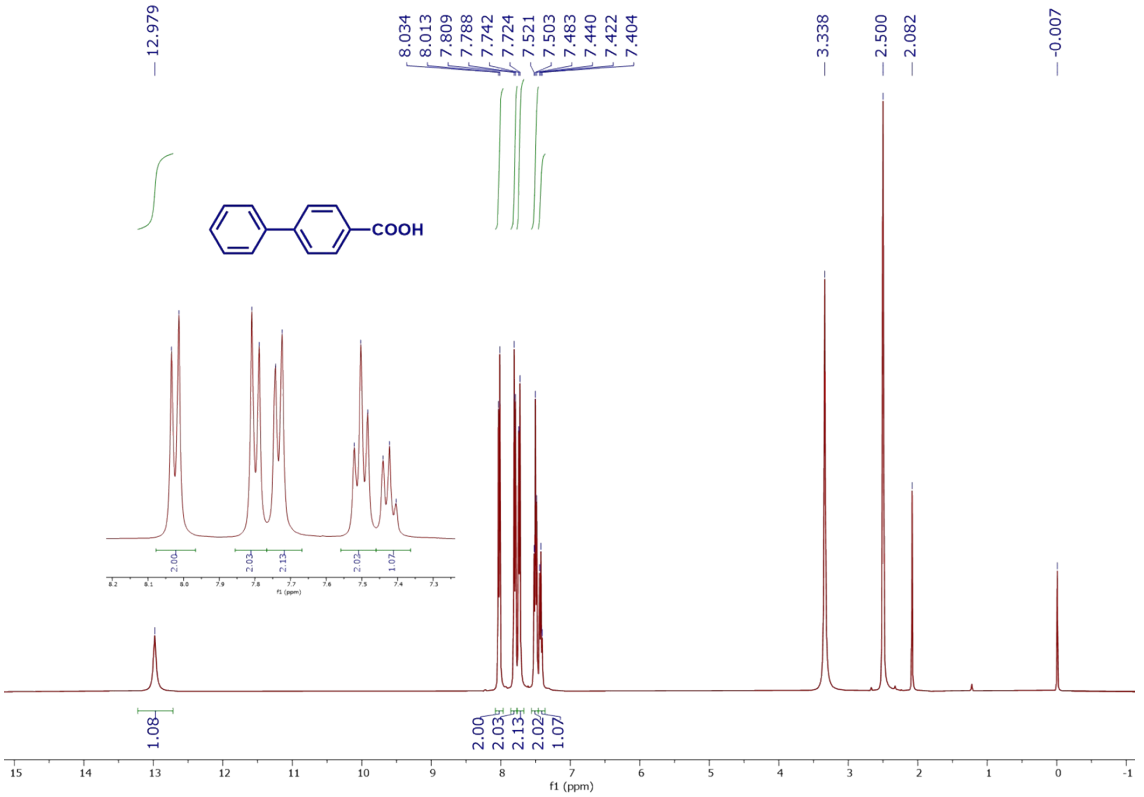

Fig. S34: ^{1}H NMR spectrum of biphenyl-4-carboxylic acid (**cc-BCA**) (DMSO-D_6, 400 MHz).

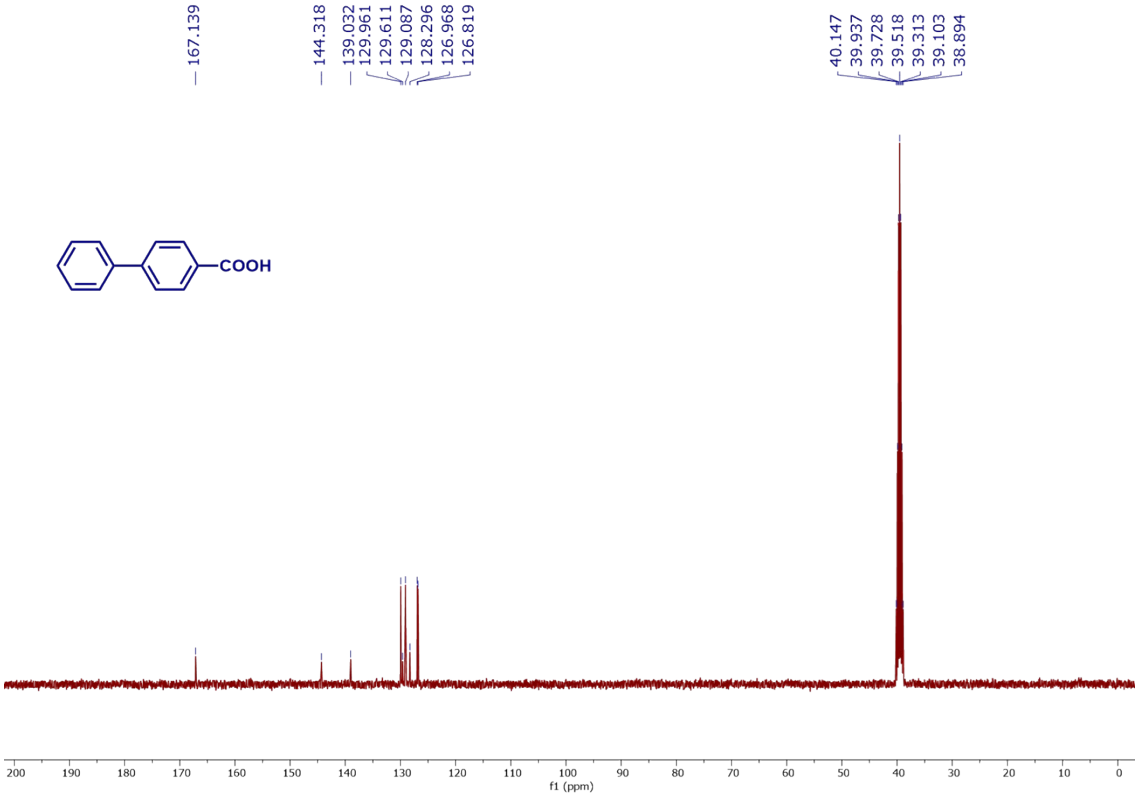

Fig. S35: ^{13}C NMR spectrum of biphenyl-4-carboxylic acid (**cc-BCA**) (DMSO-D_6, 100 MHz).

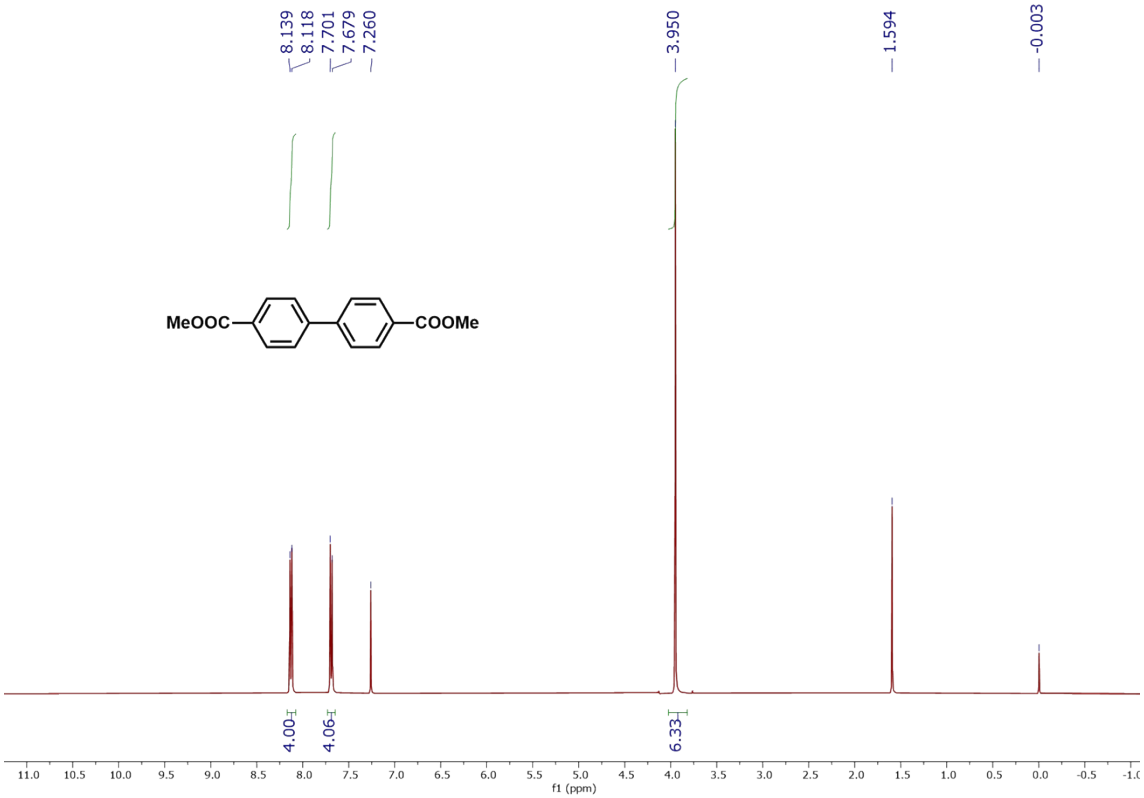

Fig. S36: ^{1}H NMR spectrum of dimethyl biphenyl-4,4′-dicarboxylate (**MBDCA**) ($CDCl_3$, 400 MHz).

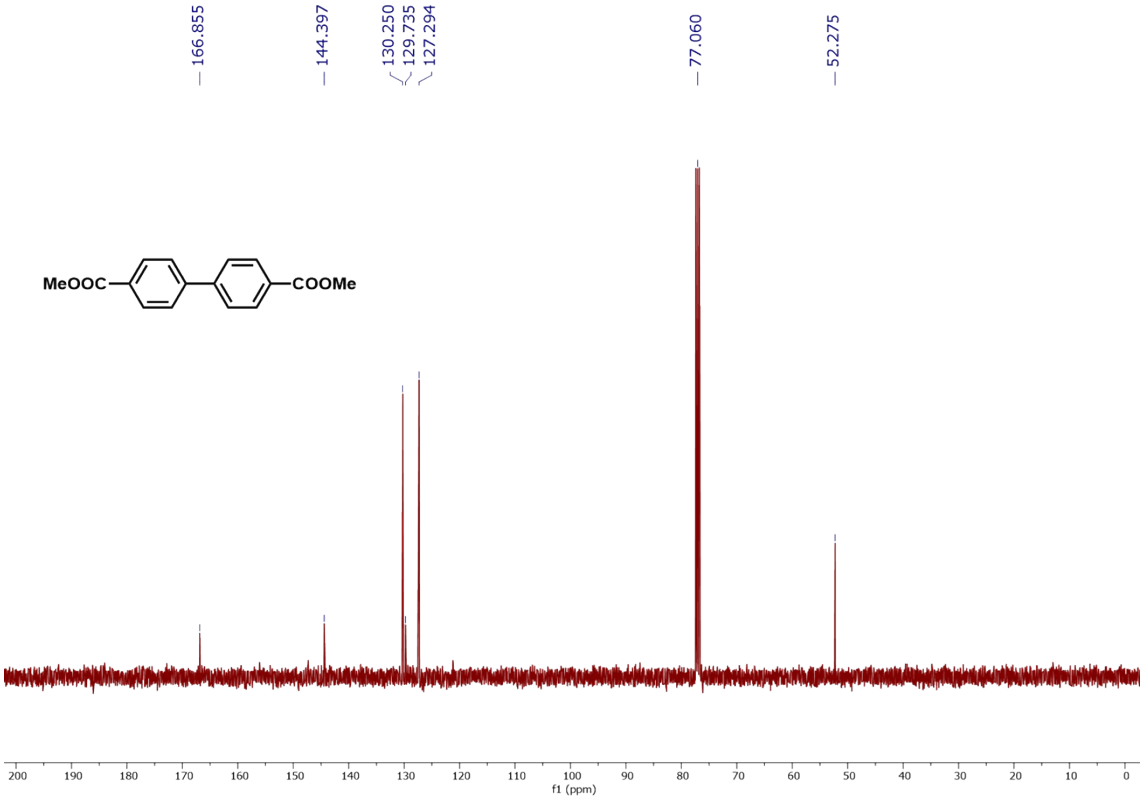

Fig. S37: ^{13}C NMR spectrum of dimethyl biphenyl-4,4′-dicarboxylate (**MBDCA**) ($CDCl_3$, 100 MHz).

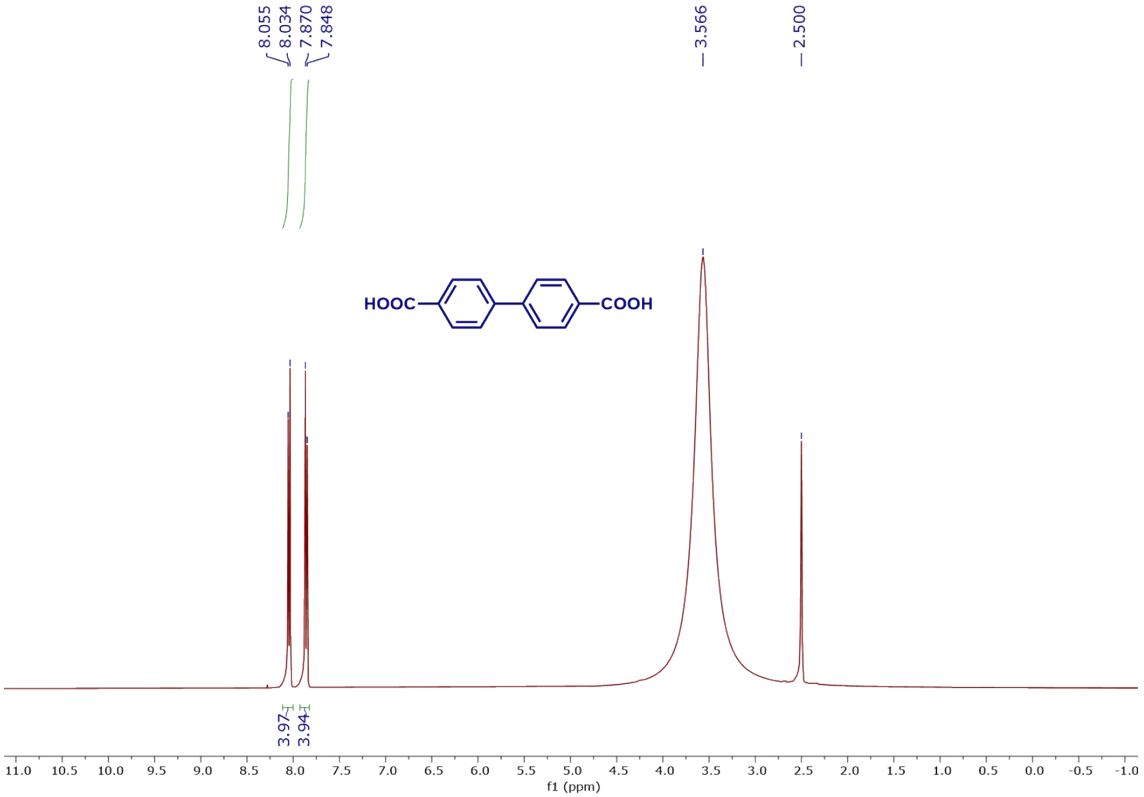

Fig. S38: ^{1}H NMR spectrum of biphenyl-4,4′-dicarboxylic acid (**cc-BDCA**) (DMSO-D_6, 400 MHz).

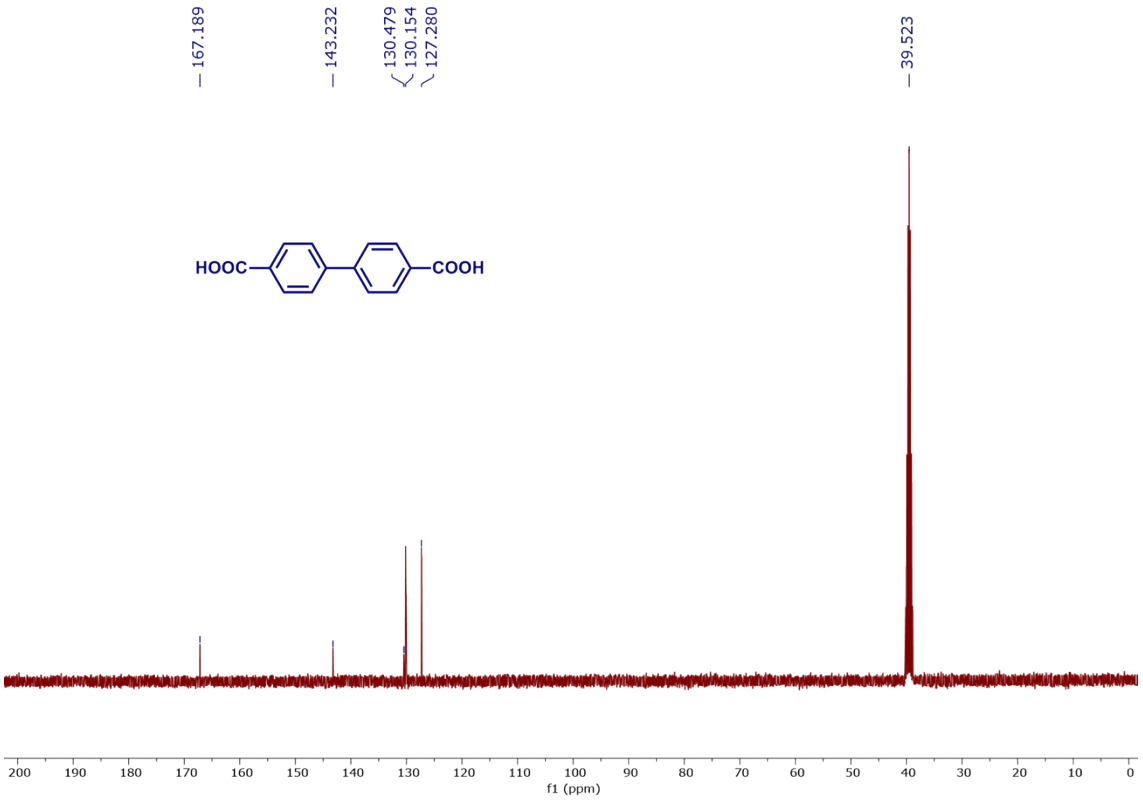

Fig. S39: ^{13}C NMR spectrum of biphenyl-4,4'-dicarboxylic acid (**cc-BDCA**) (DMSO-D_6, 100 MHz).

48. References

1. Epifanovsky *et al.*, *J. Chem. Phys.,* 2021, **155**, 084801.

2. (a) A. D. Becke, *J. Chem. Phys.,* 1993, **98**, 1372. (b) C. Lee, W. Yang and R. G. Parr, *Phys. Rev. B,* 1988, **37**, 785–789. (c) B. Miehlich, A. Savin, H. Stoll and H. Preuss, *Chem. Phys. Lett.,* 1989, **157**, 200–206.

3. G. Scalmani and M. J. Frisch, *J. Chem. Phy.,* 2010, **132**, 114110.

4. T. Yanai, D. P. Tew and N. C. Handy, *Chem. Phys. Lett.,* 2004, **393**, 51–57.

5. S. Hirata and M. Head-Gordon, *Chem. Phys. Lett.,* 1999, **314**, 291–299.

6. I. Mayer, *Chem. Phys. Lett.,* 2007, **437**, 284–286.

7. H.A. Bethe and E.E. Salpeter, Quantum Mechanics of One- and Two-Electron Atoms. New York: Plenum Press. **1977**, p. 181.

8. A.T.B. Gilbert, IQmol, http://www.iqmol.org/.

9. Sigma-Aldrich website, https://www.sigmaaldrich.com/IN/en/product/aldrich/679100, (accessed October 2025).

10. R.L. Dannley and B. Zaremsky, *J. Am. Chem. Soc.,* 1955*,* **77**, 1588–1590.

11. Sigma-Aldrich website, https://www.sigmaaldrich.com/IN/en/product/aldrich/437905, (accessed October 2025).

12. Spackman *et al.*, *J. Appl. Cryst.,* 2021, **54**, 1006–1011.